DEVELOPMENT OF THE PRESSURE-SENSITIVE-PAINT TECHNIQUE FOR ADVANCED TURBOMACHINERY APPLICATIONS

by

Kelly R. Navarra

Thesis submitted to the Faculty of the Virginia Polytechnic Institute and State University in partial fulfillment of the requirements for the degree of

MASTER OF SCIENCE

IN

MECHANICAL ENGINEERING

APPROVED BY:

Dr. W. F. O'Brien, Chair
Dr. C. A. Dancey
Dr. D. C. Rabe
Dr. J. R. Gord

April 24, 1997

Blacksburg, Virginia

DEVELOPMENT OF THE PRESSURE-SENSITIVE-PAINT TECHNIQUE FOR ADVANCED TURBOMACHINERY APPLICATIONS

by

Kelly R. Navarra

Dr. Walter F. O'Brien, Ph.D., Chairman
Department of Mechanical Engineering

(ABSTRACT)

A new pressure-measurement technique which employs the tools of molecular spectroscopy has recently received considerable attention in the fluid mechanics community. Measurements are made via oxygen-sensitive molecules attached to the surface of interest as a coating, or paint. The pressure-sensitive-paint (PSP) technique is now commonly used in stationary wind-tunnel tests; this thesis presents the extension of the technique to advanced turbomachinery applications. New pressure- and temperature-sensitive paints (TSPs) have been developed for application to a state-of-the-art transonic compressor where pressures up to 2 atm and surface temperatures up to 140° C are expected for the first-stage rotor. PSP and TSP data has been acquired from the suction surface of the first-stage rotor of a transonic compressor operating at its peak-efficiency condition. The shock structure is clearly visible in the pressure image, and visual comparison to the corresponding computational fluid dynamics (CFD) prediction shows qualitative agreement to the PSP data.

ACKNOWLEDGEMENTS

TABLE OF CONTENTS

LIST OF FIGURES

LIST OF TABLES

CHAPTER 1.0   INTRODUCTION

The turbomachinery community is continually striving to improve the performance of gas turbine engines. The engine performance depends upon the compressor pressure ratio and efficiency where the stage pressure ratio is a function of the work, inlet total temperature, and stage efficiency. The work generated by a rotor on the fluid is defined by the product of the rotor speed and the change in the tangential component of the absolute velocity between the inlet and the exit of the rotor. The stagnation pressure rise across the stage strongly depends upon the stage efficiency which is a function of the total temperature across the rotor.

The turning of the flow which creates work is induced by the pressure profile over the suction and pressure surfaces of the blade. Because the pressure is rising through the rotor passage the amount of turning is limited by blade-surface and end-wall boundary layer behavior. Boundary layers in an adverse pressure gradient tend to separate, which can cause a loss of efficiency and prevent any further increase in the pressure ratio. Currently, the stage pressure ratio and stage efficiency is determined experimentally by measuring the inlet and exit total pressure and temperature of the stage. Because of the complex flow interactions which occur in a rotor, it would be most beneficial to also know the pressure profile of the blade surface.

Early surface pressure measurements of a subsonic rotor were made by Sexton, O'Brien, and Moses in 1973 where blade-mounted pressure transducers and a multi-channel radio telemetry system were used (1). Still today, blade-mounted pressure transducers are the only means to measure surface pressure on rotors. Unfortunately, such transducers cover a limited region ($< 5\%$) of the blade surface, result in some compromise to the structural integrity of the blade and to the flow integrity, and have limited reliability in full-scale transonic turbomachinery environments. For these reasons, improved blade-surface pressure-measurement techniques are needed to aid the understanding of flow behavior in turbomachinery components.

A relatively new technique that employs the tools of molecular spectroscopy to measure pressures by optical means is the subject of this thesis. Measurements are made via photoluminescent oxygen-sensitive molecules attached to the surface of interest as a coating, or paint; hence, the technology is referred to as pressure-sensitive paint (PSP). Although a number of PSPs are currently available, they were engineered for use in stationary wind-tunnel tests and do not meet the pressure and temperature requirements of turbomachinery applications. The objective of this research effort was to develop a PSP suitable for the turbomachinery environment and to demonstrate the measurement technique for turbomachinery applications.

This thesis begins with a brief discussion of the theory of luminescence and dynamic quenching, followed by a presentation of the general method of acquiring data from the oxygen-sensitive molecules (lumiphores). Subsequent sections discuss the establishment of paint-performance requirements for turbomachinery applications, procedures for evaluating various paints, and performance results of the paints developed during this research effort. The remaining

sections describe the application of the developed technology to a state-of-the-art transonic compressor. Quantitative results acquired from the suction surface of the first-stage rotor of a transonic compressor are presented. These results are discussed, and future work planned for this research area are identified.

CHAPTER 2.0   BACKGROUND

Photoluminescence was first used as a tool for optical pressure sensing in 1980 by Peterson and Fitzgerald (2). Unfortunately, the significance of the experiment was dismissed because the oxygen sensitivity of the fluorescent dye and the oxygen permeability of the binding medium were poor. Over the following decade, paint performance improved, charge-couple-device (CCD) cameras evolved, and digital hardware advanced to a level where the use of photoluminescence to obtain optical surface-pressure measurements became practical (3).

Early development of the pressure-sensitive paint (PSP) technique for external aerodynamics was initiated at the Central Aero-Hydrodynamics Institute in Moscow (TsAGI) and the University of Moscow in the mid-1980's (4,5,6). TsAGI developed a commercial PSP system jointly with the Italian firm INTECO (7,8). European researchers such as the Deutsche Forschungsanstalt fur Luft-und Raumfahrt e.V. (DLR) began PSP efforts using the INTECO system but have since initiated an independent PSP program (9,10). Also, TsAGI recently formed OPTROD, Ltd., to market their paint formulations (11,12) in a venture separate from INTECO. Other independent PSP efforts in Europe now include British Aerospace (13) and the Office National d'Etudes et de Recherches Aérospatiales (ONERA) (14).

In the United States, McLachlan and Bell at NASA Ames Research Center, in collaboration with the University of Washington, have made contributions to development of the technique since the late 1980's (15-20). Efforts were also initiated at McDonnell Douglas Aerospace in 1990 (3,21,22), followed by Purdue University (23,24,25) and NASA Langley (26,27) in the early 1990's. In the mid-1990's the University of Florida began a program related to the McDonnell Douglas effort (28,29). Around this time, Arnold Engineering Development Center (AEDC) (30), Wright Laboratory (WL) (31), and NASA Lewis (32) initiated paint programs. Undoubtedly, there are many other programs which now exist as the number of organizations interested in PSP steadily increases due to the attractiveness of its high-spatial resolution and low-cost.

CHAPTER 3.0   MEASUREMENT CONCEPT

Knowledge of the relationship that exists between the luminescence of particular molecules and the oxygen concentration dates back to the late 1930's (33). Since the measured oxygen concentration is directly related to the partial pressure of air at a given temperature,

pressure can be accurately determined based upon the luminescence behavior of these molecules. Although this tool has been used primarily in the biomedical field, engineers now apply the technology to aerodynamic surfaces to acquire global pressure measurements of aerodynamic surfaces. To date, numerous studies have been conducted in efforts to better understand and utilize luminescence quenching. A discussion of the relationship among these luminescent molecules, oxygen concentration, and local pressure follows.
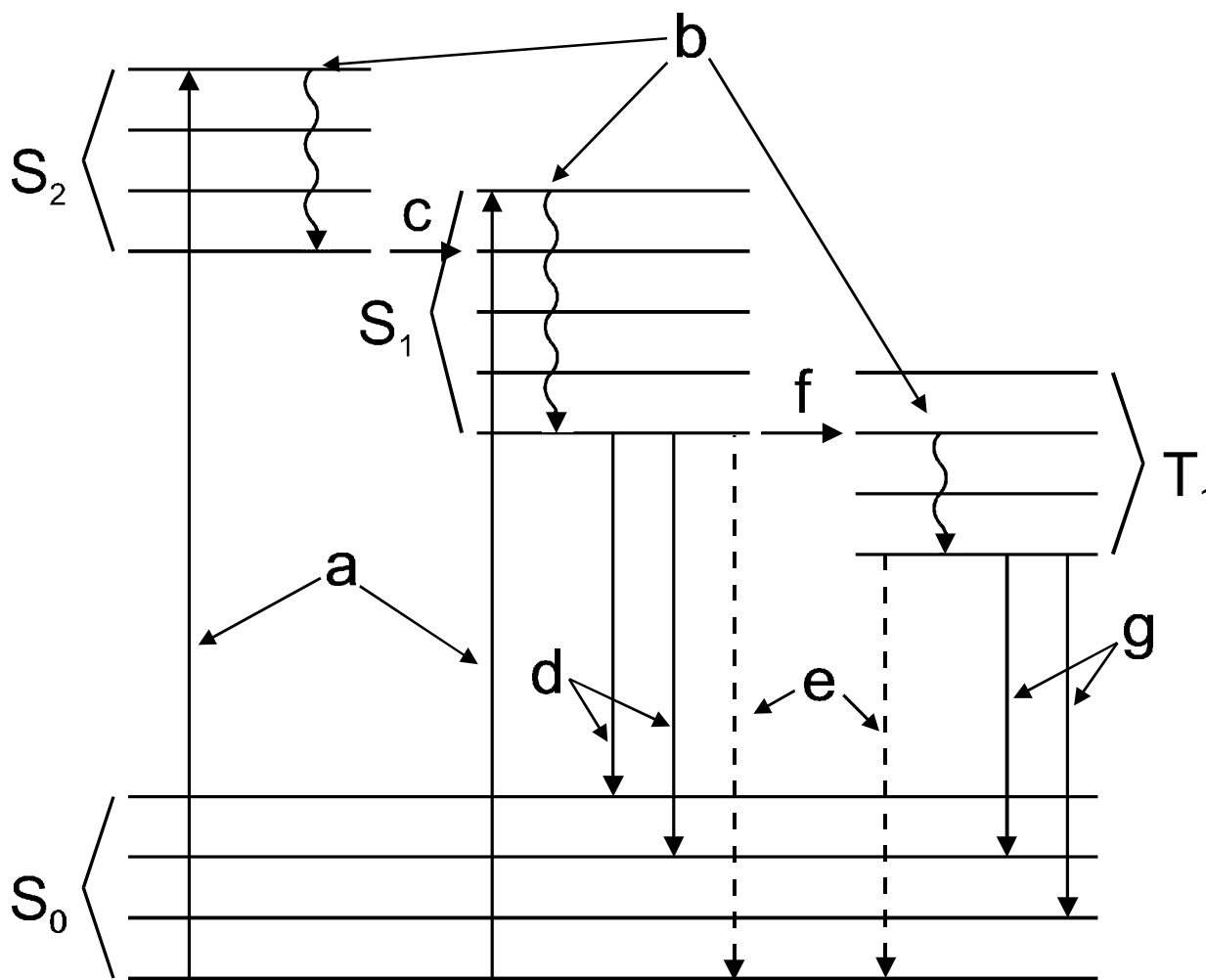

FIGURE 3.1 Jablonski diagram depicting the vibrational and electronic states and the photophysical processes associated with a typical lumiphore (from reference 34).

3.1   Luminescence

Two luminescence processes, phosphorescence and fluorescence, can be effectively used to measure oxygen concentration. Each of these is described in the context of the Jablonski energy-level diagram for a typical lumiphore, as depicted in Fig. 3.1 (34). The electronic energy states are the manifolds labeled S_0, T_1 etc.; multiple vibrational energy levels exist within each electronic state. Figure 3.1 is arranged to display electronic states and vibrational energy levels, with lower-energy states appearing at the bottom of the figure and higher-energy states appearing at the top. The rest of this section will describe the relevant photophysical processes associated with a typical oxygen-measurement sequence through the use of this diagram.

Absorption (a) occurs when the lumiphore is exposed to electromagnetic radiation of appropriate energy (i.e., frequency). During this process electrons are promoted from the ground vibrational energy level of the S_0 electronic state to excited vibrational energy levels in the S_1 and/or the S_2 electronic state. Higher-lying excited electronic states may be populated as well but only those shown in Fig. 3.1 are required to discuss the processes involved in oxygen quenching. Once in an excited state, the lumiphore may undergo a number of processes to return to its stable, lowest-energy configuration. These deactivation processes can be broadly grouped into two general categories: 1) non-radiative deactivation processes in which the excess energy associated with the absorbed photon is transferred to the surrounding medium, and 2) radiative deactivation processes in which the excess energy is emitted as light.

Immediately following the absorption or excitation event (a), the excited lumiphore relaxes to the lowest-energy vibrational level of the excited electronic state (S_1 and/or S_2) through vibrational relaxation, depicted by the wavy line labeled (b), in which excess vibrational energy associated with the lumiphore is transferred to the thermal motion of the surrounding medium. Vibrational relaxation in the S_2 electronic state (or in higher-lying excited electronic states) is followed by internal conversion (c) to lower-lying excited electronic states. This non-radiative process couples states of the same multiplicity (multiplicity describes the number of unpaired electrons associated with a particular energy state). In this example S_1 and S_2 are singlet states, i.e., states in which the valence electrons are fully paired. Through non-radiative sequences of internal conversion and vibrational relaxation, the excited lumiphore rapidly relaxes to the lowest vibrational state of the S_1-excited electronic state.

From this energy state, the molecule may undergo a number of different processes. Under some circumstances internal conversion to the ground electronic state, S_0, with subsequent vibrational relaxation is an important deactivation mechanism. However, fluorescence (d) and external conversion (e) through dynamic quenching are the key processes associated with measurements based on PSPs. Fluorescence is a radiative (luminescent) process that couples states of the same multiplicity ($S_1 \rightarrow S_0$). During this process excess energy is emitted as photons to yield lumiphores in the ground electronic state. External conversion (dynamic quenching) is a non-radiative process that competes with fluorescence for deactivation of the S_1 excited electronic state. Specifically, dynamic quenching is the transfer of energy from the excited-state lumiphore

to another non-luminescent molecule, or "quencher", through collision. Without the presence of a quencher, all of the excess excited-state energy of the lumiphore is dissipated through fluorescence; generating the highest intensity level. With the presence of a quencher, however, this fluorescence intensity is reduced because part of the excess energy is transferred to the quenching molecules through dynamic quenching. Quenching of the lumiphore will continue with increased quencher concentration until all fluorescence is eliminated. Thus, the competition between dynamic quenching and fluorescence permits the determination of the quencher concentration. A mathematical representation of dynamic quenching is presented in Appendix A.

There are many classes of lumiphores which are quenched by a variety of species such as oxygen, carbon dioxide, and pH (35). The lumiphores used for pressure-sensitive paints, for example, are quenched by oxygen molecules, hence, "oxygen quenching". While the common reference to the paints being *pressure* sensitive is technically inaccurate the name clearly indicates the resulting measurement. The methods used to relate the measured oxygen concentration to the local pressure is addressed later in Section 4.0.

It is important to recognize that many lumiphores do not deactivate by means of fluorescence. Some S_1-excited state lumiphores undergo intersystem crossing (f)--a process in which the excited singlet state couples to a triplet state, T_1. This event involves a change in multiplicity from the singlet state where the valence electrons are fully paired to a triplet state where two electrons are unpaired. The vibrationally relaxed T_1 state can couple to S_0 through intersystem crossing, external conversion (dynamic quenching), or phosphorescence (g). The first two processes are non-radiative, while the last involves photon emission. Once again, the competition between oxygen quenching and phosphorescence can be used to measure oxygen concentration. Therefore, the PSP technique can utilize either fluorescence or phosphorescence as the underlying mechanism to measure the oxygen concentration.

It should be noted that the wavelength emission by either fluorescence or phosphorescence is related to the change in the energy between the excited state and the ground state. While all the lumiphores will relax to the ground electronic state, they all may not relax to the same vibrational energy level within the ground state. Similarly, the lumiphores may not be excited to the same electronic state or vibrational energy level. Therefore, the absorption and emission spectra of luminescent molecules generally cover a range of wavelengths; the emission wavelengths are red-shifted due to the energy dissipated through non-radiative mechanisms. Similarly, phosphorescence emission wavelengths are red-shifted compared to fluorescence emission wavelengths because the phosphorescence process utilizes lower-lying energy states than fluorescence.

It is also important to note that the Jablonski diagram and the photophysical processes identified in this discussion best describe the typical characteristics of lumiphores in liquid solution. While it provides an excellent description of the spectroscopic behavior of luminescent molecules, this model should be applied with caution to the prediction of the behavior of specific

PSP formulations; lumiphores immobilized in solid matrices can display somewhat different characteristics.

3.2   Fluorescence vs. Phosphorescence

Several important differences exist in the underlying photophysics associated with fluorescence and phosphorescence. Specific differences in these processes, aside from the spectral characteristics previously mentioned, involve timescales, sensitivities to dynamic quenching, and sensitivities to temperature. Each of these luminescence processes has advantages and disadvantages when used for optical pressure measurements.

The events that result in fluorescence emission involve spectroscopic transitions that occur between states of the same multiplicity; the lumiphore does not have to alter its number of unpaired electrons in order to relax to the lower electronic state where fluorescence can occur. As a result, the timescale (lifetime) for spontaneous fluorescence typically ranges from 10^{-10} to 10^{-6} s (34). Phosphorescence, on the other hand, involves transitions that require a change in multiplicity; transitions from a singlet state where the electrons are fully paired to a triplet state where two electrons are unpaired. Therefore, the lumiphore must break apart one electron pair, change the spin of an electron, and form two unpaired electrons before it can relax to the triplet electronic state. Because this has to occur twice, in the triplet formation ($S_1 \rightarrow T_1$) and in the triplet deactivation ($T_1 \rightarrow S_0$), phosphorescence typically occurs on a timescale ranging from 10^{-4} to 10^4 s as a consequence of this spectroscopic requirement (34). This enormous difference in emission timescales has significant implications for the application of optical pressure-measurement techniques to the study of transient or unsteady phenomena.

It is also important to note the effects of differences in dynamic quenching on these processes. Quenching (labeled (e) in Fig. 3.1) deactivates S_1 to compete with fluorescence (d) and deactivates T_1 to compete with phosphorescence (g). Because of the long timescales associated with phosphorescence, dynamic quenching that occurs at a given rate has a more pronounced effect on a phosphorescence signal than on a fluorescence signal. The long lifetime of the T_1-excited electronic state increases the likelihood that quenching collisions will take place. In other words, quenching competes more effectively with the slower phosphorescence process than with the faster fluorescence process.

These differences in sensitivity to dynamic quenching have two important implications. First, the phosphorescent measurement of oxygen concentration--and, therefore, pressure--is more sensitive than fluorescent measurement. For a given change in oxygen concentration, the change in phosphorescence intensity is greater than that in fluorescence intensity. As a result, phosphorescence measurements permit the experimental resolution of smaller changes in absolute pressure. The second implication involves the effects of temperature on the two processes. As with oxygen concentration, dynamic quenching rates increase with temperature. As a result both fluorescence   and   phosphorescence   are   sensitive   to   temperature;   however,   because

phosphorescence is more sensitive to dynamic quenching than fluorescence it is also more sensitive to fluctuations in temperature. In a paint formulation designed for the measurement of temperature fields, this is a desirable quality; however, this sensitivity to temperature is problematic when relating the measured oxygen concentration to pressure.

CHAPTER 4.0   MEASUREMENT TECHNIQUE

According to Ingle and Crouch (34), the fraction of absorbed photons which are converted to luminescence photons is defined by the luminescence quantum efficiency, ϕ_L:

$$\phi_L = \frac{k_L}{k_L + k_C + k_f + k_q[Q]} \tag{1}$$

where Q is the concentration of the quencher, k refers to rates and the subscripts L, c, f, and q refer to luminescence, internal conversion, intersystem crossing, and quenching, respectively, as depicted in Fig. 3.1. The rate of quenching is largely diffusion controlled and depends upon the temperature and viscosity of the surroundings. If the luminescence is fluorescent, then k_f equals zero (intersystem crossing does not occur) and the L subscript can be replaced with F to indicate fluorescence. Phosphorescence involves all the processes presented in Fig. 3.1 and the subscript L in equation 1 can be replaced with P to indicate phosphorescence. For the present derivation the luminescence process will remain unspecified. The luminescence quantum efficiency in the absence of quenching is given by:

$$\phi_{L_0} = \frac{k_L}{k_L + k_C + k_f} \tag{2}$$

where the subscript 0 denotes the absence of quenching. The Stern-Volmer equation is derived through the ratio of equations 1 and 2:

$$\frac{\phi}{\phi_0} = \frac{I}{I_0} = 1 + \frac{k_q[Q]}{k_L + k_C + k_f} \tag{3a}$$

$$\frac{I}{I_0} = 1 + \tau_0 k_q[Q] \tag{3b}$$

$$\frac{I}{I_0} = 1 + K_{SV}[Q] \tag{3c}$$

where I is the integrated intensity, τ_0 is the decay time of the luminescence (lifetime) in the absence of oxygen, and the product of k_q and τ_0 is the Stern-Volmer constant, K_{SV}. The presence of τ_0 in equation 3b quantitatively describes why phosphorescent molecules are generally more sensitive to oxygen concentration (for a given k_q) than fluorescent molecules, as pointed out in Section 3.2 (phosphorescence involves longer timescales). A plot of the Stern-Volmer equation (3c) should yield a straight line, however, deviations from the ideal behavior are sometimes observed when the extent of quenching is large (34).

Application of this Stern-Volmer model requires the luminescence intensity in the absence of oxygen (I_0) to be measured, which is not feasible in some laboratory experiments. The need for I_0 can be eliminated by taking the ratio of two different environmental conditions. In practice, a reference condition (wind-off) is used where the pressure and temperature distributions are constant and equal to atmospheric conditions. The run condition (wind-on) is the case where the pressure and temperature distributions are unknown. The wind-off condition is divided by the wind-on image as follows:

$$\frac{\dfrac{I}{I_0}}{\dfrac{I_0}{I_{REF}}} = \frac{1 + K_{SV}\dfrac{P}{RT}}{1 + K_{SV}\dfrac{P_{REF}}{RT_{REF}}} \tag{4a}$$

$$\frac{I}{I_{REF}} = A(T) + B(T)\frac{PT_{REF}}{TP_{REF}} \tag{4b}$$

$$A(T) = \frac{1}{1 + K_{SV}\dfrac{P_{REF}}{RT_{REF}}} \tag{4c}$$

$$B(T) = \frac{K_{SV}}{1 + K_{SV}\dfrac{P_{REF}}{RT_{REF}}}(\frac{P_{REF}}{RT_{REF}}) \tag{4d}$$

where the oxygen concentration is substituted with the ideal gas law $Q = n/v = P/RT$, where R is the specific gas constant, P is the pressure and T is the temperature. A and B are coefficients which are temperature dependent as a result of the temperature dependence of the Stern-Volmer constant. The ratio of the luminescence intensities I and I_{REF} not only provides the desired pressure-oxygen concentration relationship but also effectively eliminates signal dependence associated with non-uniformity of the lumiphore concentration in the paint layer and non-uniform illumination.

8

Intensities are generally sampled over the area of interest using some type of detector array such as a charge-coupled-device (CCD) camera or photomultiplier tube (PMT). The output of the array can be visually represented as an image, with the luminescence intensity displayed in gray scale or pseudo-color. In many of the applications reported in references 3-32, the temperatures are assumed constant between the two conditions and T_{REF} cancels T in equation 4b. However, this constant-temperature assumption is not valid for most aerodynamic applications, and, as a result, knowledge of the surface temperature is required to determine the surface pressure.

CHAPTER 5.0   PAINT DEVELOPMENT FOR TURBOMACHINERY APPLICATION

Based upon previous experience using PSP in rotors (discussed in Appendix B), it was recognized that the goal of extending the usefulness of this new measurement technique to steady-state applications in turbomachinery could not be achieved until paint performance was improved. Needed improvements included the extension of the operational pressure and temperature range-- with adequate pressure resolution to resolve flow phenomena. The paint must also adhere to the blade and provide an adequate signal-to-noise ratio (SNR). Table 5.1 shows the first-stage rotor design condition and airfoil geometry parameters of a full-scale transonic compressor (36). In the following paragraphs, the paint-performance requirements for acquiring quantitative data from this state-of-the-art transonic compressor are identified.

Table 5.1   First-stage-rotor design condition and airfoil geometry parameters from reference 36.

Parameter	Value
Design Speed	13,288 rpm
Total Pressure Ratio	2.5
Total Temperature Ratio	1.3
Mass Flow	71.8 kg/sec
Rotor Radius	0.3524 m
Number of Blades	16
Average Aspect Ratio	1.22
Inlet Radius Ratio	0.33
Average Radius Ratio	0.47
Tip Solidity	1.5
Max. Thickness/Chord	0.028

5.1   Luminescence Decay Time

For a rotating environment, the luminescence decay time (lifetime) of the paint is important. This issue surfaces with the timing requirements associated with imaging a rotating blade or when the flow phenomenon being measured is transient, or both. In the case of turbomachinery, the time of the excitation and the subsequent lifetime of the paint must occur within the data acquisition time (gate time) required to image the rotating blade. The intensity of a lumiphore is inversely proportional to $e^{-k_q*Q(t)}$ (see Appendix A). Therefore, to collect photons over 99% of the decay, the gate time should be $\sim 5\tau_0$. On the other hand, the gate time required to image the blade motion for a 1-mm spatial resolution is < 2 μs based on the data presented in Table 5.1, as calculated in Appendix A. Therefore, the paint in this particular application must contain a lumiphore with a lifetime of < 400 ns. With phosphorescent lifetimes typically ranging from 10^{-4} to 10^4 s, as stated previously, fluorescent compounds must be used (10^{-10} to 10^{-6} s) for compatibility with the timing requirements for a high-speed turbomachinery blade application (34).

5.2   Pressure and Temperature Range

Figure 5.1 shows the computational-fluid-dynamics (CFD) prediction of the pressure on the suction surface of the first-stage rotor at 85% corrected speed (Nc) under the peak-efficiency test condition. The CFD code used was developed by NASA Lewis (37). These data were evaluated to define the required paint-performance range of 0.3 - 2 atm and -10 to +140° C. Of these two requirements, the temperature is more difficult to achieve because many common lumiphores cannot survive beyond 100° C. As mentioned in Section 3.2, the rate of quenching, k_q, is diffusion controlled and depends upon the temperature and viscosity of the surroundings, i.e. the viscosity and the oxygen diffusivity of the binder. Although minimization of the temperature dependence of the PSP is a design goal, it is unlikely a paint which is completely insensitive to temperature can be developed.

If the temperature gradient is small, a gross temperature correction can be used to produce acceptable results. However, applications with large temperature gradients, such as in turbomachinery, require a temperature-sensitive paint, or other temperature-sensing technique, that will allow more detailed temperature corrections. Several organizations are investigating the development of a dual-lumiphore paint where pressure and temperature can be measured simultaneously. However, a dual-lumiphore paint is not necessary for turbomachinery application where multiple blades can be painted--assuming each blade experiences the same flow field at the imaging location. Therefore, a separate temperature-sensitive paint (TSP) was also developed to provide a means to temperature-correct the PSP.
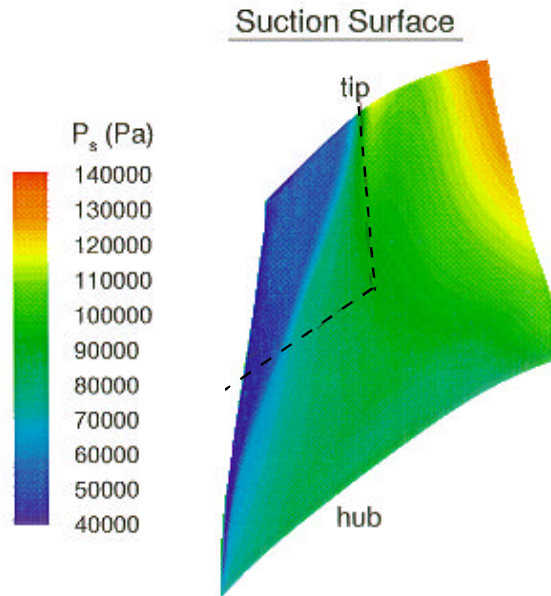
Figure 5.1 CFD surface-pressure prediction at 85% Nc, peak-efficiency operating condition.

5.3 Spatial and Pressure Resolution

The ultimate goal of PSP development would be to provide a measurement having higher spatial and pressure resolution than is currently available with blade-mounted pressure transducers. The issue of spatial resolution is really no contest. When pressure transducers are used, very few are mounted (<5% of the blade area) on blades because of the high cost and risk of compromise to the structural integrity of the blade and the flow integrity. In the case of PSP, the spatial resolution is limited only by the detection device. With current CCD cameras having a million or more pixels, PSP provides unequaled spatial resolution.

To define the performance requirements of PSP in the area of pressure resolution, the state-of-the art of blade-mounted pressure transducers was assessed. A recent application of blade-mounted pressure transducers to a transonic compressor is reported in references 38 and 39. Here, the data-reduction process provided pressure measurements having resolutions of 3.17 kPa (38). Thus, to compete with pressure transducers, PSP must provide pressure measurements with a resolution < 3.17 kPa. Measurements in pressure to 0.34 kPa (0.05 psi) have been reported using PSPs (40). However, this resolution was obtained in a well-controlled test environment, whereas in most applications model movement and temperature gradients significantly affect the measurement errors. Table 5.2 summarizes the paint-performance requirements defined in this section.

Table 5.2 Pressure-sensitive paint requirements for the first-stage transonic rotor presented in Table 5.1.

Parameter	Value
Pressure Range	0.3 to 2.0 atmospheres
Temperature Range	-10 to 140 °C
Gate Time for Imaging*	<2 μs
Lifetime	<400 ns (requires fluorescence)
Spatial Resolution	1 mm
Pressure Resolution	<3.17 kPa

*Depends on rotor speed and desired spatial resolution.

CHAPTER 6.0   PAINT EVALUATION AND PERFORMANCE

Several PSPs are currently available. However, these paints were engineered for stationary wind-tunnel applications that do not have critical timing requirements for imaging the test surface. Therefore, most of these paints utilize phosphorescence--despite the increased temperature sensitivity--to take advantage of the increased sensitivity to pressure resulting from the long luminescent decay of phosphorescence. As discussed earlier, turbomachinery requires the short decay time of fluorescent materials. Therefore, a fluorescent PSP is required for turbomachinery applications and a fluorescent TSP is also needed to provide a means for temperature-correcting the PSP data.

Based upon its routine use for oxygen sensing in the medical field, the lumiphore selected for PSP development was pyrene. Bis-pyrenal propane, a commonly used laser dye which is not quenched by oxygen, was selected for TSP development. The bis-pyrenal propane was an ideal choice to use with pyrene because both of these fluorescent molecules can be excited using the same light source (337 nm); however, a blue filter is required for the bis-pyrenal propane to filter out wavelengths in the emission band which are not temperature sensitive. In a vacuum pyrene has a lifetime of 323.5 ns at room temperature and the bis-pyrenal propane has a lifetime of 186.8 ns at room temperature. The PSP lifetime value is largest at vacuum, as predicted in Appendix A.

The pressure- or temperature-sensitive paint is made by mixing the respective lumiphore with a binding solution which is immediately applied to the surface of interest and allowed to dry. Interactions can occur between the lumiphore and the binding medium. Therefore, care must be taken to select a binding medium which does not reduce the oxygen sensing capability of the lumiphore. With the current lack of understanding of these interactions (41), the selection of a

suitable binder is mostly trial and error. Thus, the process of developing a new T/PSP involves the Stern-Volmer calibration of numerous binder/lumiphore combinations to determine the sensitivity over the desired pressure and temperature range. The following paragraphs describe the calibration procedure used to evaluate the performance of TSP and PSP formulations.

6.1   Paint Calibration Procedure

The pressure and temperature characteristics of the PSPs are dictated by the parametric Stern-Volmer relation described in equation 4b. The calibration coefficients, A and B, were experimentally determined with the use of a vacuum chamber. The chamber employed in this study was the cross pipe shown schematically in Fig. 6.1. Quartz windows were located in two orthogonal flanges. A portion of the nitrogen laser beam (337 nm, 300 μJ, 3-ns pulse at 29 Hz) was split to trigger the digital oscilloscope by means of a photodiode. A mirror was used to turn the remainder of the beam (62 nJ) to impinge on the paint sample through the first quartz window. The sample was mounted at ~45 deg and the resulting fluorescence exited through the second window. The sample was slightly offset from 45 deg to minimize the laser scatter to the detector by deviating the laser reflection from the detector path. The fluorescence passed through an ultra violet filter to remove any remaining laser scatter. If the sample was the TSP, then a blue filter was placed behind the ultra violet filter to remove the emission band of photons which were not temperature sensitive. Collection optics were used to gather the fluorescence and a photomultiplier tube (PMT) was used to detect the fluorescence intensity over time (decay). The PMT produced a trace of the decay on the sampling oscilloscope. A neutral density filter was required in the beam path to reduce the signal intensity to prevent saturation of the PMT.

A computer was used to establish the pressure and temperature environment of the calibration chamber by means of a digital pressure controller and thermal-electric temperature controller. The paint sample was mounted on the thermal-electric device (TED), and two set screws fitted with ceramic sleeves were used to secure the paint sample. Thermal compound was used to provide good heat transfer between the paint sample and the TED. A K-type thermocouple was placed in contact with the paint surface between the sample and one of the ceramic sleeves. Again, thermal compound was used to provide sufficient heat transfer. The pressure of the calibration unit could be varied from 10 kPa to 199 kPa, and the surface temperature of the sample could be varied from -15° C to 150° C.

For determining the Stern-Volmer relation, the calibration unit was run by a computer program. The user input the desired pressure and temperature range over which the sample would be tested and indicated the number of data points and the number of traces to average for each point; this was typically set to 128 traces. The temperature controller maintained the temperature while the pressure was varied. Once traces were acquired over the desired pressure range, the temperature was changed and traces were again acquired over the desired pressure range. For each temperature a data file was created in which the temperature, the pressure

readings, and the corresponding integrated intensity of the trace were recorded. A full calibration consisted of 20 pressures ranging from 10 kPa to 199 kPa and 30 temperatures ranging from -10° C to 150° C. The entire 600-point calibration required ~ 2 hr for completion.

Figure 6.1 Paint calibration chamber.

As reported in Section 4.0, deviations from the ideal behavior are sometimes observed when the extent of quenching is large (34). Most PSPs calibrated over a range of 0 to 1 atm do follow the linear Stern-Volmer model (see Fig. C.1); however, extension of the pressure range results in reduced sensitivity. Therefore, a second-order curve fit is required to sufficiently model the data.

One characteristic of oxygen concentration previously mentioned is temperature sensitivity. The temperature sensitivity of the oxygen concentration is well understood for lumiphores in solutions and the rate constants which make up K_{SV} (see equations 3a-3c) have been well characterized (34). However, the complex interaction between the lumiphore and the binder hinders the development of accurate rate models for lumiphores suspended in solids. Several

organizations currently research this very important, yet extremely difficult subject (41-44). Due to the extreme quenching which occurs beyond one atm and the lack of accurate rate-constant models, the ideal Stern-Volmer model must be abandoned and the relation between the intensity ratio and pressure (and temperature) must be parametrically determined. The same stands for the TSP despite its independence of quenching.

6.2   Paint Calibration Results

Through the use of the calibration chamber, new PSP and TSP formulas better suited for turbomachinery applications were developed. Numerous paint formulations composed of various binders and solvents were tested as well as methods of application and surface treatments. The following paragraphs present the paints developed for the intended application.

The first PSP developed for turbomachinery, which employed pyrene, displayed a complete and irreversible loss of pressure sensitivity above 80° C. Development continued in an attempt to increase the temperature capability of the paint. It was concluded that the loss of pressure sensitivity above 80° C was a result of the vaporization of the pyrene. Therefore, the approach used to increase the temperature capability of the paint was to identify fluorescent probe molecules with higher boiling points compared with pyrene's boiling point of 150° C. Acid forms of pyrene were found to have boiling points higher than pure pyrene; 1-pyrene-acetic acid, 1-pyrene-butyric acid and 1-pyrene-carboxylic acid have boiling points of 211° C, 185° C, and 271° C, respectively (45). The paint employing pyrene-acetic acid (PAA) was selected for the rotor test because the paint displayed superior performance. The calibration of the PAA paint is shown in Fig. 6.2. As the figure shows, the PAA-PSP survived temperatures to 150° C and pressures to 200 kPa (~2 atm). The lifetime of the paint at room temperature was determined to be 323.5 ns in a vacuum.

The effect of temperature on the rate constants presented in equations 3a-3c is apparent in the data presented. The relationship between the surface pressure and the resulting paint luminescence was modeled for each temperature using a second-order polynomial curve fit. The relationships between the surface temperature and the resulting A, B, and C coefficients were then modeled using a third-order polynomial curve fit. Four independent samples were calibrated to assess the sample-to-sample variation of the PSP; results are shown in Fig. 6.3 at room temperature. The mean value and the standard deviation of the independent calibration results were then determined from the four samples. In general, the PSP displayed a 10% variation in the calibration coefficients from application to application for the data shown in Fig. 6.3.

$$P = A(T) + B(T)I_R + C(T)I_R^2$$

$$A(T) = a_1 + a_2 T + a_3 T^2 + a_4 T^3$$

$$B(T) = b_1 + b_2 T + b_3 T^2 + b_4 T^3$$

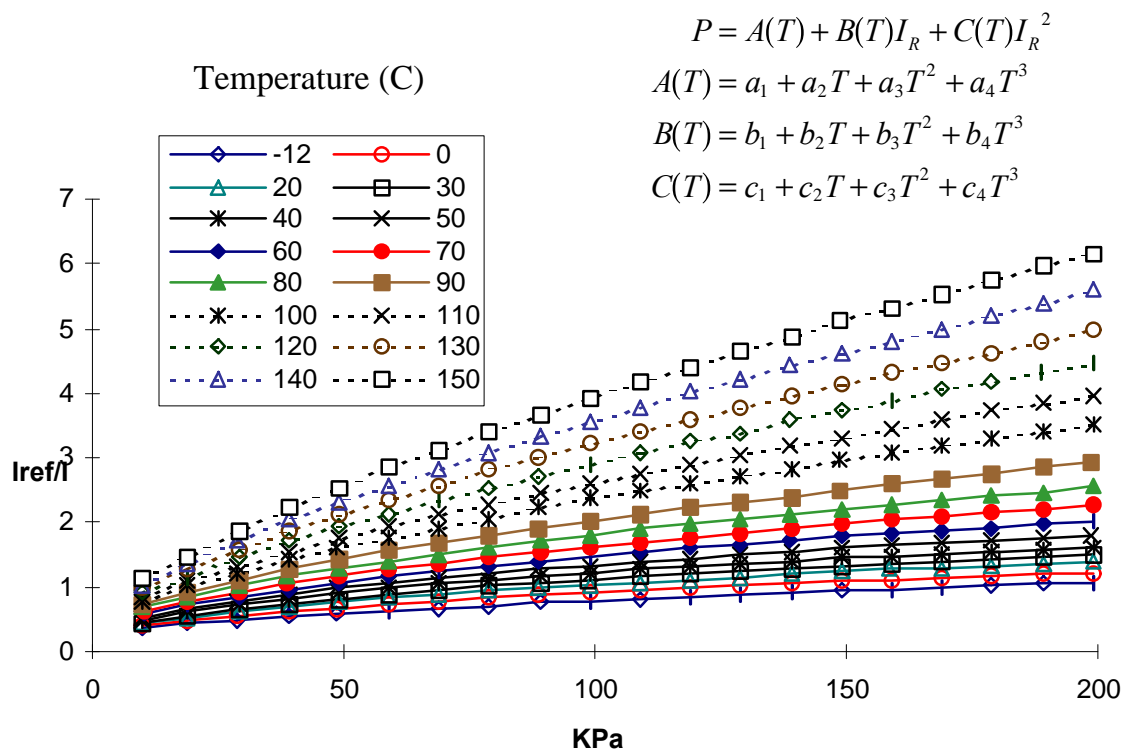$$C(T) = c_1 + c_2 T + c_3 T^2 + c_4 T^3$$

Figure 6.2 Performance of the PSP employing pyrene-acetic acid (I_R=Iref/I).
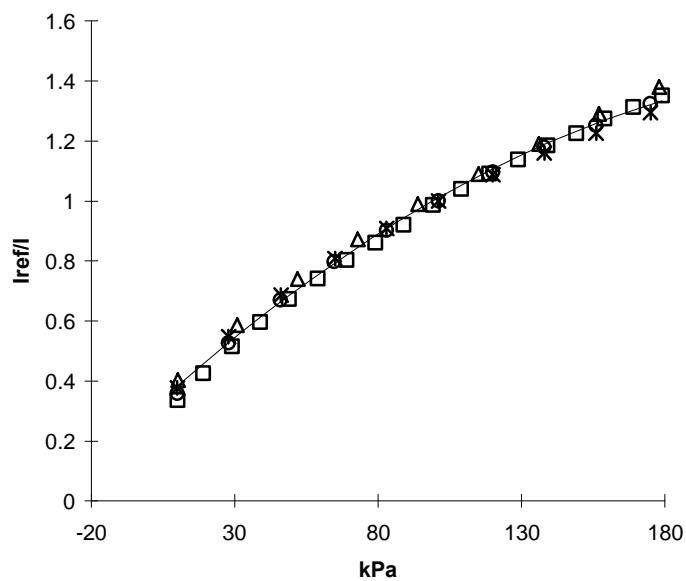
Figure 6.3 Calibration variation of four independent PSP samples at room temperature.

The TSP developed to correct for the PSP temperature sensitivity proved suitable for the rotor test, as shown in Fig. 6.4. As in Fig. 6.3, the data presented in Fig. 6.4 represent the calibration of four independent TSP samples. A second-order polynomial curve fit was used to model the relationship between the surface temperature and the paint luminescence. Because the TSP is insensitive to pressure, no further modeling was required. The TSP displayed an 8% variation in the calibration coefficients from application to application. These results indicate that both the PSP and TSP must be calibrated for each application to account for the application to application variation.
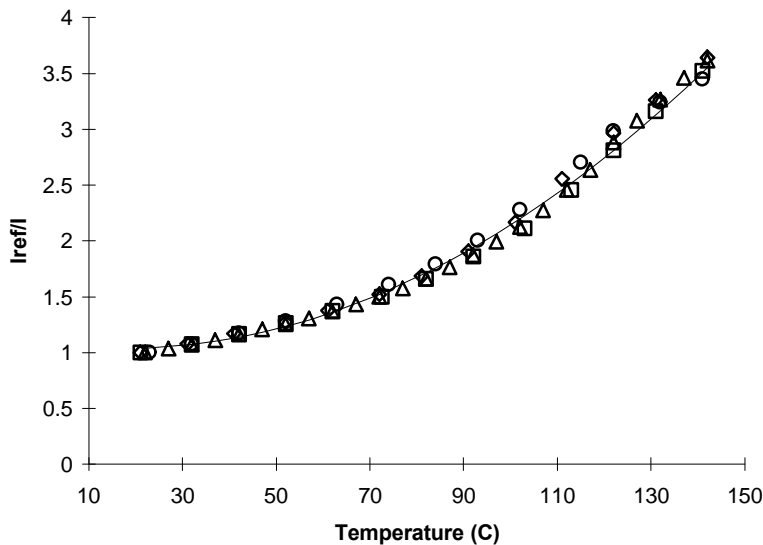

Figure 6.4 Performance of TSP developed for turbomachinery.

6.3 Paint Photodegradation

All luminescence-based paints display a common characteristic referred to as photodegradation, whereby the paint-intensity signal deteriorates as a function of time with continued exposure of the paint to visible light. The calibration chamber was used to characterize the rate of photodegradation of the paints as a function of energy. The energy of the laser beam impinging on the paint surface was measured at 62 nJ with a 1.5-ns pulse at a repetition rate of 29 Hz. Intensity measurements were acquired from each paint for a minimum of 30 mJ of applied energy. Figures 6.5 and 6.6 show the photodegradation results of the PSP and TSP as a function of input energy. The paint photodegradation is expressed in terms of percent of the initial intensity. In general, the PSP displayed a higher rate of degradation than the TSP and absorbed a larger amount of input energy before the rate started to decline. At 30 mJ of total energy

delivered to the paint the PSP degraded ~ 6.6% while the TSP degraded ~ 1.3%. The rate of photodegradation circumvents the advantage of using increased illumination power to improve signal levels. Hence, the effect of photodegradation must be considered when designing a PSP experiment.
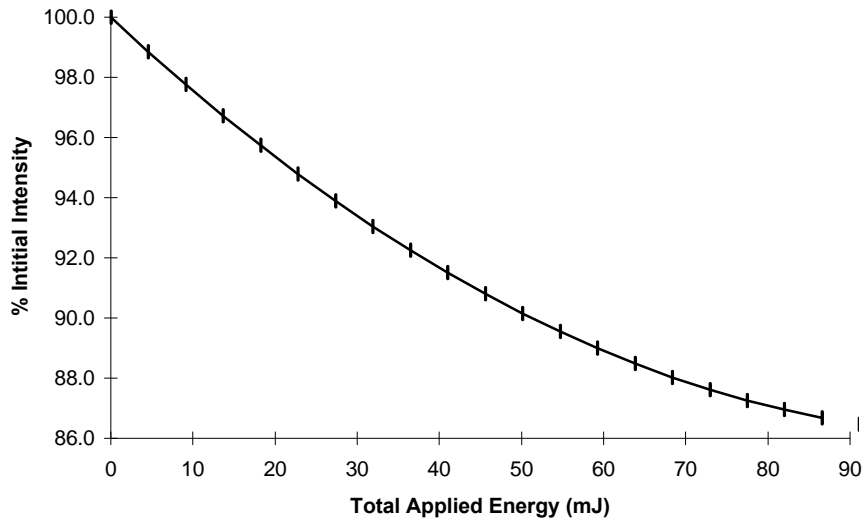

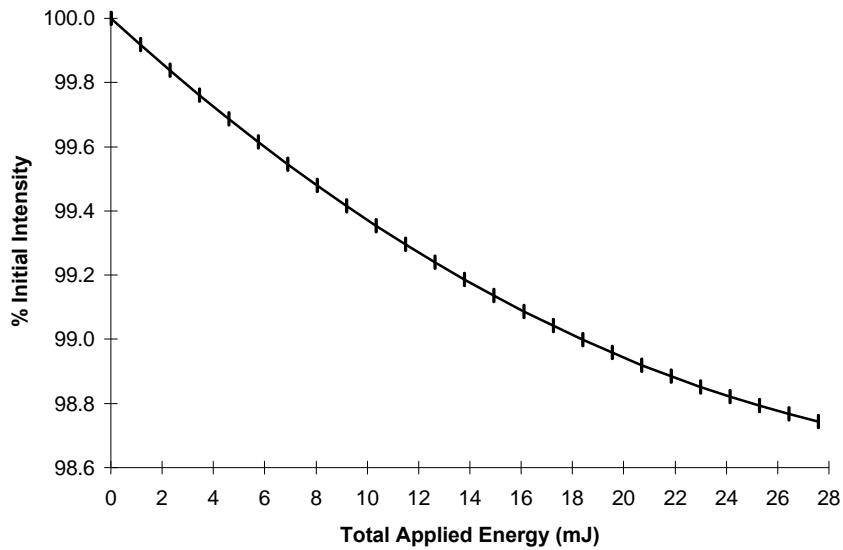**Figure 6.5** PSP rate of photodegradation as a function of total energy delivered to the paint.

Figure 6.6 TSP rate of photodegradation as a function of total energy delivered to the paint.

6.4   Effect of Oil on Paint Performance

Because of the complexity of full-scale test facilities such as the Turbine Engine Research Facility (TERC), "non-ideal" testing conditions are often encountered. For example, oil residue is a common occurrence in a compressor test. This is a potential problem for PSP and TSP measurements because most oils fluoresce. If the oil changes the reference intensity of the painted surface, pre-test wind-off images used in post-processing are invalid. In a worst-case scenario, the oil could hinder the permeation of oxygen through the surface, inhibiting the pressure-sensing capability of the paint. Thus, it was important to investigate the effects of oil on the paint surface.

A simple experiment was conducted using the calibration chamber to investigate the effect of oil on the PSP. Figure 6.7 shows three calibrations of the same paint sample. First a fresh, clean sample was calibrated. Oil was then dripped on the sample which was re-calibrated. Finally, the sample was rinsed with alcohol to demonstrate a potential cleaning method and calibrated a third time.
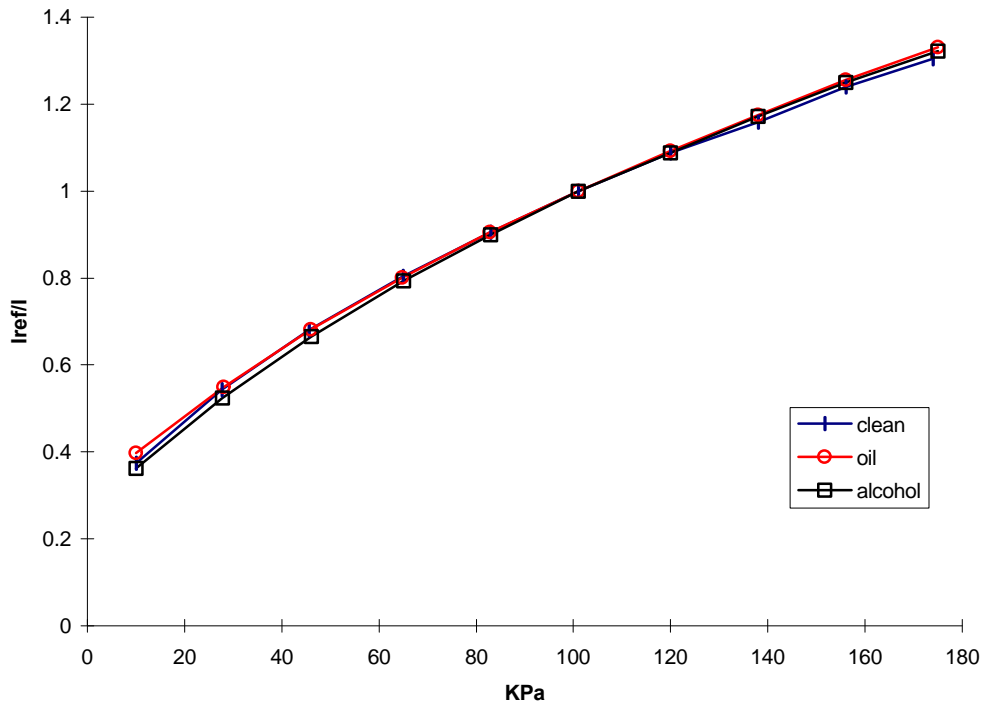

Figure 6.7 Effect of Oil on PSP performance.

While the absolute intensity of the paint with and without oil varied ~2%, the relative change (referenced to a point which also contained oil) in the intensity, as indicated in Figure 6.7, was negligibly affected by the oil. However, it is important that the wind-off and wind-on images represent the same effects; problems were anticipated in the event where one image (either the wind-off or wind-on) contained oil and the other did not. Therefore, it was recommended that wind-off images be acquired before and after a test; any changes in these images would represent photodegradation and the presence of oil. This comparison should help identify the errors associated with the data.

CHAPTER 7.0   APPLICATION TO A TRANSONIC ROTOR

For demonstration of the application, the selected pressure- and temperature-sensitive paints were applied to a state-of-the-art transonic compressor. The compressor test was conducted during the period of September 1996 to January 1997 at the Turbine Engine Research Facility (TERC) at Wright Laboratory. A detailed description of the TERC is given in Appendix D. The primary objective of this test was to obtain quantitative pressure measurements from the suction surface of the first-stage rotor. The following paragraphs present a description of the test-article, the painting procedure, the test setup, and data-acquisition and post-processing procedures.

Figure 7.1 Test-article schematic.

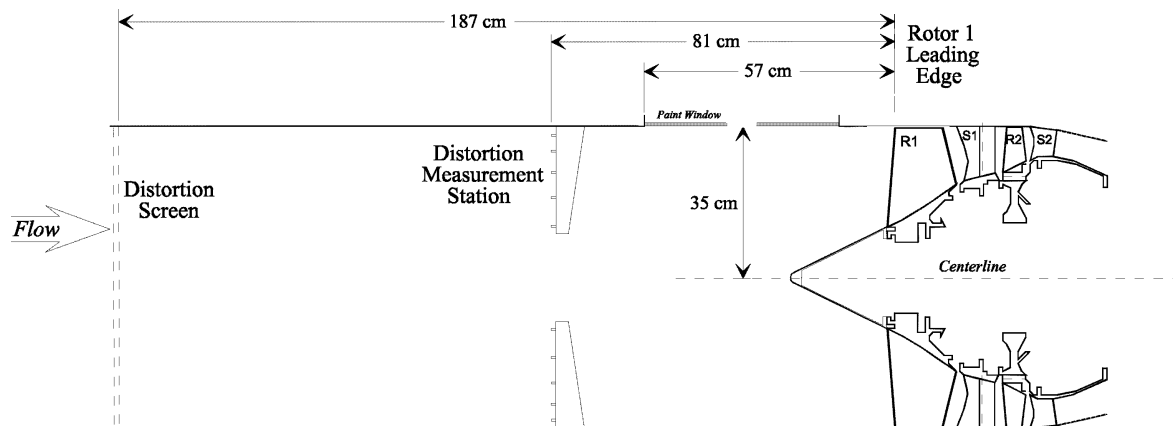## 7.1   Test-Article Description/Preparation

The test article was the two-stage low-aspect-ratio transonic compressor shown schematically in Fig. 7.1. This compressor has been tested several times at the TERC; therefore, a large volume of data is available such as Laser-Doppler-Velocimeter (LDV), distortion, and pressure-transducer results (36,38,39). The first-stage-rotor design condition and airfoil

geometry parameters were previously presented in Table 5.1, and the CFD prediction for surface pressure were presented in Fig. 5.1.

Various time constraints made it necessary to paint the rotor in place. The casing was removed prior to painting to allow better access. The blades were first cleaned with acetone using a lint-free cloth; a clear Dow Corning 1200 Primer Coat was then applied and allowed to dry for a minimum of 6 hr to improve adhesion of the PSP to the blade. Fresh paint solutions were then mixed and applied to the blades using a commercial artist air brush. Both the temperature and pressure paints were dry to the touch in ~ 1 hr, but 8 hr were required for the paint to fully cure. Extreme caution was taken to minimize the exposure of the paint to room light to prevent photodegradation. Figure 7.2 shows a painted blade. In the figure, conventional strain gage instrumentation is visible on the two preceding blades.

Figure 7.2 Photograph of painted transonic-compressor blade.

After 1 hr of drying time, the alignment marks were applied to the painted blades to provide regions of zero intensity in the data images. These marks play an important role in post-processing where they are used to align the wind-off and wind-on images. This is especially important in turbomachinery applications where the blade twist changes between stationary and rotating conditions. In previous paint tests, as reported in Appendix B, quantitative measurement data were not obtained primarily because of the inadequate alignment of these images.

Three alignment-mark requirements were identified. First, the alignment marks must be of sufficient size (2-3 pixels) to be located in each image. Second, a minimum of twelve marks are necessary to perform the highest order mapping (if required) of the wind-off to the wind-on image

during post processing (described in Section 7.5). Due to expected twist in the blade, it was anticipated that the highest order mapping (third-order polynomial) would be required to properly align the wind-off and wind-on images. Any alignment marks in addition to the basic twelve would improve the mapping of these images. Thus, it was desired to have 24 or more alignment marks on each blade. Finally, the marks should be located in similar known locations on each painted blade since a temperature-corrected pressure image could be obtained only if the temperature- and pressure-painted blades were aligned. The measured locations of the marks on the blades were also used to determine the scale of the final images. For positioning the alignment marks, a paper template was used to measure 33 alignment-mark positions on the blade. Holes ~ 1.6 mm in diameter were punched into the template at these locations and the marks were applied to the painted blades using a fine-point permanent marker.

Figure 7.3 Transonic-rotor PSP test setup.
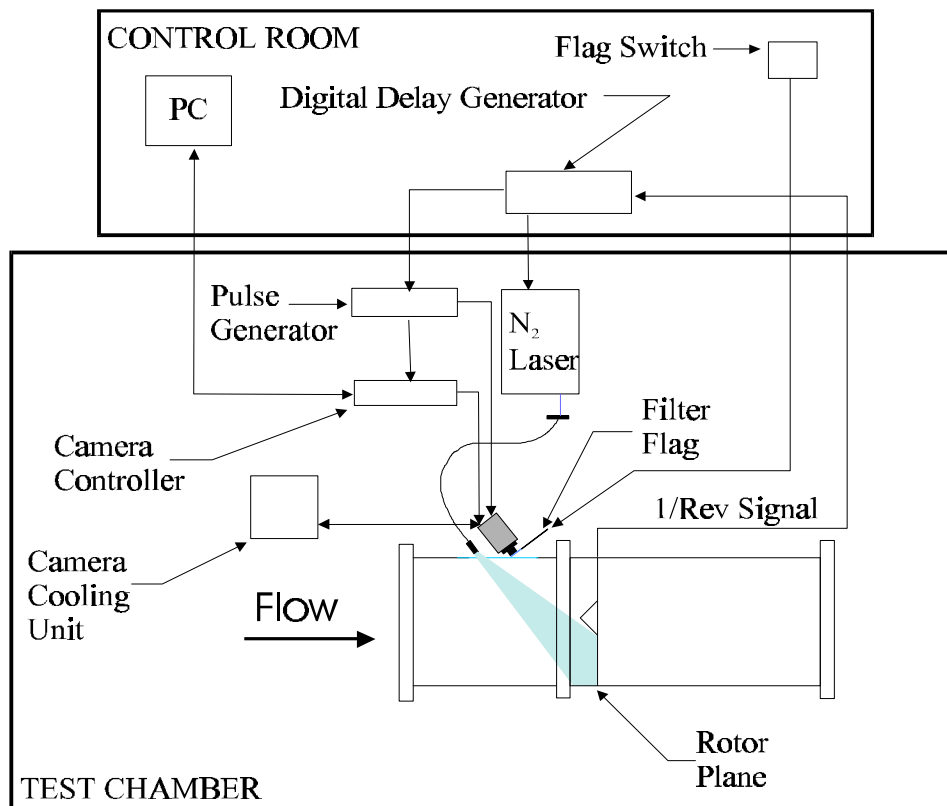
7.2   Test Setup

The rotor test setup is shown in Fig. 7.3. A 305 x 25 mm window was placed ~260 mm upstream of the rotor leading edge. A 16-bit Princeton Instruments intensified charge-coupled device (ICCD) camera (576 x 384-pixel Thompson chip), fitted with a 50-mm f/1.2 lens, was located ~0.5 m upstream of the rotor. The camera viewed the blades across the flow path and

was angled ~5 deg below the centerline to avoid viewing the bullet nose. A 2-mJ nitrogen pulsed laser beam (337 nm, 1-ns pulse) was launched into a fiber which was mounted adjacent to the camera. The laser was used in the pulse-on-demand mode—the laser only fired when the command was given to the ICCD to acquire an image. The beam (measured at 0.4 µJ at the exit of the fiber) was expanded to illuminate the visible suction surface of the first-stage rotor. With the presented viewing angle, the adjacent blade prevented viewing beyond 52% chord at the tip, and the image size restricted viewing inboard of 62% span.

The Princeton Instruments detection system included the ICCD, an ST-138 camera controller for image acquisition and readout via the personal computer, and an FG-100 pulse generator for triggering the camera. The camera system and laser were mounted on an optical table inside the test chamber. A Neslab cooling unit was used to maintain the ICCD chip at -20° C to minimize readout noise. The camera and nitrogen laser were remotely controlled from an adjacent room. As mentioned previously, TSP requires a blue filter on the detector while PSP does not. A filter arm (flag) was configured with a switch to allow remote positioning of the blue filter. When switched on, the current in the flag created a magnetic field which attracted the flag towards another magnet mounted on the optical table. Thus, the switch could be used to move the filter in and out of the camera path. Figure 7.4 is a photograph of the described test setup.
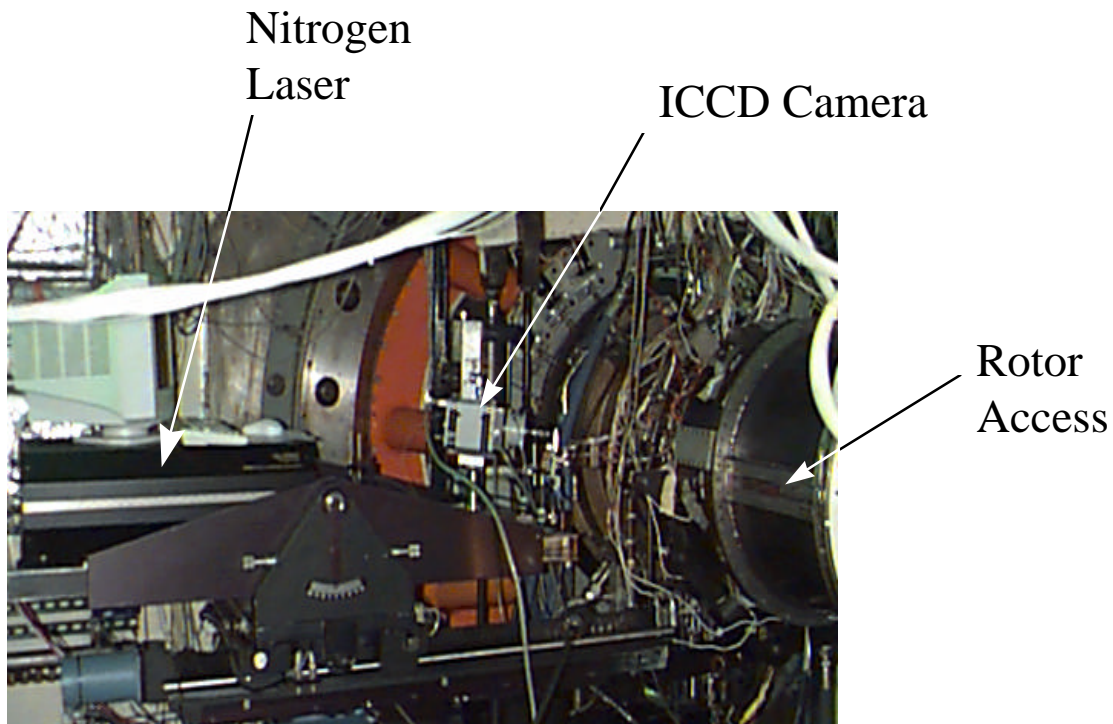

Figure 7.4 Photograph of the test setup.

7.3   Paint Calibration/Test Differences

The external calibrations of the paints obtained from the calibration chamber were applied to the images acquired in the rotor experiment to obtain values for surface pressure and temperature. Therefore, it is important to address potential differences between the calibration and the rotor experiment. These differences include the laser illumination, the detection device used to measure intensity, and the viewing angle of the painted surface. Each of these issues will be addressed in the following paragraphs.

Illumination

Both the calibration chamber and the rotor experiment used a nitrogen laser at 337 nm. The calibration chamber used a smaller laser which delivered 62 nJ to the sample surface for every 1.5 ns-pulse. The pulse rate of this laser was typically set to 29 Hz. The laser used in the rotor test produced 0.4 μJ at the exit of the optical fiber and had a 1-ns-pulse width. Because the laser pulse widths were approximately equal and both were considerably shorter than the maximum lifetime of the PSP (in a vacuum ~323.5 ns; TSP at room temperature is 186.8 ns), no deconvolution of the emitted signal was required.

The energy differences were also considered between the two lasers. The calibration chamber was used to characterize the rate of photodegradation of the paints in terms of input energy, as presented in Section 6.3. With the laser used in the experiment being more powerful than that used in the calibration chamber, acceleration of the paint photodegradation was a potential problem. To minimize the unnecessary exposure of the paint, the laser in the rotor experiment was used in the pulse-on-demand mode where the laser only fired when the operator acquired an image. The 0.4 μJ beam was expanded to cover ~18,250 mm^2 of the blade applying approximately 11.1 nJ to the paint surface for each image. Based upon the photodegradation data presented previously, the acquisition of 450 images would result in a 0.7% degradation of the TSP and a 2.7% degradation of the PSP. Regardless of the number of images acquired, knowledge of the relationship between power and photodegradation provided a means to account for the degradation throughout the course of the test, if desired.

Detector

Three characteristics of the photo-detector must be considered between the calibration chamber and the experimental test setup. The first characteristic is the spectral response of the detector. Both the ICCD used in the rotor test and the photomultiplier tube (PMT) used in the calibration chamber use the same s-4 photocathode. Therefore, the spectral characteristics are identical.

Other considerations are the linear range and the sensitivity of each detector. Figure 7.5 will be used to address both of these considerations. The figure presents calibrations of the same PSP sample at room temperature from both the ICCD camera and the calibration chamber (PMT). For the ICCD, ten images were acquired at each pressure. A computer program was then used to determine the average intensity over a 150x150 pixel region and to compute the standard deviation of the ten images. As can be seen in Figure 7.5, the error bars associated with the ICCD calibration suggest that the SNR of the PMT is superior to that of the ICCD camera; the error bars expand with increasing pressure because the intensity level, I, decreases with pressure. However, the averaged intensity ratios from the ICCD are equivalent indicating that a sensitivity comparable to that of a PMT can be obtained if a minimum of 10 images are averaged to compute the intensity ratio.

Figure 7.5 PSP calibration at room temperature using both the ICCD and the PMT.

Figure 7.5 also indicates that the linear range of the ICCD is comparable to that of the PMT. However, the drop in the last data point of the ICCD acquired at 199 kPa hints to the beginning of a deviation of the linear range for this particular ICCD. For the pressure range of interest, the sensitivity and the linear range of the ICCD and the PMT are essentially equal. Therefore, the calibration data obtained using the PMT can be directly used to process the PSP and TSP images acquired using the ICCD. A minimum of ten images must be acquired for each test condition to adequately assess the extreme low-level intensities of the high-pressure regions.

The final difference between the calibration chamber and the rotor experiment which should be considered is the viewing angle. In the calibration chamber the focused laser beam impinged the paint sample at ~ 45 deg and the PMT was also at a 45 deg angle from the sample (~ 90 deg from the laser). In the rotor experiment the ICCD viewed the blade at ~ 64 deg and the laser was offset from the camera ~10 deg. The incidence of the laser is irrelevant unless the laser light is reflected directly back into the detector. Normally, perpendicular illumination is avoided to prevent such an occurrence. As for the detection of the paint luminescence, Lambert's Law states that the luminescence intensity emitted in any direction from a luminescent surface varies as the cosine of the angle between the normal to the surface and the direction of the luminescence (46). The luminescence intensity of the surface is, therefore, independent of direction. Also, called the Lambert Law of Cosines, the viewing angle of the painted object generally does not effect the measurement unless the viewing angle is very shallow.

7.4   Data-Acquisition Procedure

The following procedure was used to image the blade and acquire data images. Once the operator sends the command to initiate image acquisition, the CCD camera was charged, and the once-per-revolution pulse (1/rev) from the test article was used to initiate the timing sequence. The 1/rev signal was delayed by the amount, Δt_{delay}, required to rotate the desired painted blade into the image plane. A Stanford Research DG535 delay generator, triggered by the 1/rev, was used to send out two pulses--the first to trigger the pulse generator, which in turn triggered the camera, and the second to trigger the laser. The second pulse trailed the first by 13 μs to take into account the time required for the camera electronics to respond to the trigger. This allowed synchronization of the arrival of the laser light at the blade surface and the activation of the camera intensifier for collecting the resulting fluorescence emission. The period of operation of the intensifier (gate time) was determined by the laser pulse width and subsequent fluorescence emission of the paint. For this test a 1-ns laser pulse was used, and the maximum fluorescence lifetime was determined from calibration to be 323.5 ns (at vacuum and room temperature). The gate time was selected to be 10 μs to take into account laser jitter on the order of 1 μs. Therefore, the timing required to image the blade (< 2 μs) was achieved by the combination of the short laser pulse and the short-lived fluorescence of the paint--not by the gate of the intensifier. The camera "shutter," or charge time, was preset to a minimum of one rotor revolution. After the shutter closed, the acquisition of another image could not be initiated until the CCD downloaded the data to the computer. The readout time of the 221,184-pixel CCD chip was 234 ms. This limits this particular camera to steady state measurements since another image can not be acquired until the readout is complete.

Four types of images were required in PSP and TSP measurements: a wind-off reference image, a wind-on test image, a black image, and a white image. The black images were taken

with the lens cap on to define the thermal noise of the CCD array. The white image was taken of a uniformly illuminated surface of arbitrary intensity. This image provided a flat-field correction for the "honeycomb" pattern on each image which results from the "minifier"--the tapered fiber-optic coupling between the photocathode and the CCD chip. Both the black and white images were only camera-dependent and could be taken either before or after the test. Thus, during a scheduled testing period, only the wind-off and wind-on images were acquired.

Wind-off images were acquired both before and after each test; pre- and post-test wind-off images could be compared to determine whether oil might be present in the compressor and to check for paint photodegradation. For acquiring the wind-off images, the rotor rotated 150 rpm where the pressure gradient was well below the current resolving capability of the paints. This approach provided valid reference images while allowing the timing circuitry to be used for accurate positioning of the blade images. For acquiring the wind-off images, the camera shutter was set to 400 ms. Sequential images were acquired using various timing delays until the desired painted blade appeared in the image. Care was taken to determine the delays required to place the TSP and PSP blades in the same location. The locations were determined by the image pixel coordinates of the blade leading edge. The delay and coordinates of each blade were recorded. Fifty wind-off images were acquired for each paint for steady-state averaging.

Once the wind-off images were acquired, the compressor was throttled to a desired test speed and condition. For the wind-on images, the camera shutter was reduced to 50 ms. To provide a constant background noise from image to image, the shutter value remained constant for all of the wind-on images, regardless of the rotational speed. From the coordinates previously recorded during the acquisition of the wind-off images, the delays required to superimpose the TSP and PSP blades were determined, and the corresponding wind-on images were acquired. Fifty wind-on images were acquired from each blade at each test condition for averaging.

7.5   Post-Processing Procedure

The post-processing was carried out mainly using PAINTCP, a program developed for NASA Ames by Sterling Software, Inc (47). This package is used in PSP image analysis for wind-tunnel aircraft model tests. For the purposes of this experiment, many of the functions within the code were not required; however, the program was used for its ability to register the alignment marks in each image and transform the wind-off image to align it with the wind-on image. A separate computer program was used to perform basic functions such as image averaging, subtraction, and division.

Each image captured by the ICCD camera can be described as a product of camera sensitivity, $S(x,y)$, illumination power, $P(x,y)$, and the paint emission, $E(x,y)$, plus thermal background noise, $B(x,y)$, as follows:

$$I(x, y) = S(x, y)P(x, y)E(x, y) + B(x, y) \qquad (5)$$

where each parameter varies spatially. As a result of equation 5, two corrections were required for the wind-off and wind-on images prior to division and conversion to quantitative temperature or pressure data: 1) a background correction to take into account the thermal noise on the ICCD chip, and 2) a flat-field correction to take into account the spatial variations in camera sensitivity and illumination (attenuation). The thermal noise was removed by subtracting the background image, which only contained $B(x,y)$, from the wind-off and wind-on images. Removal of the camera attenuation was more difficult. A flat-field correction was used to remove the attenuation caused by the minifier--which results in a honeycomb pattern on the data image. This pattern--a mechanical effect of the camera--was fixed in all images; therefore, manipulation of the wind-on image to align it with the wind-off image would skew this pattern relative to the wind-on image, adding unnecessary pattern noise to the final image, as illustrated in Fig. 7.6.
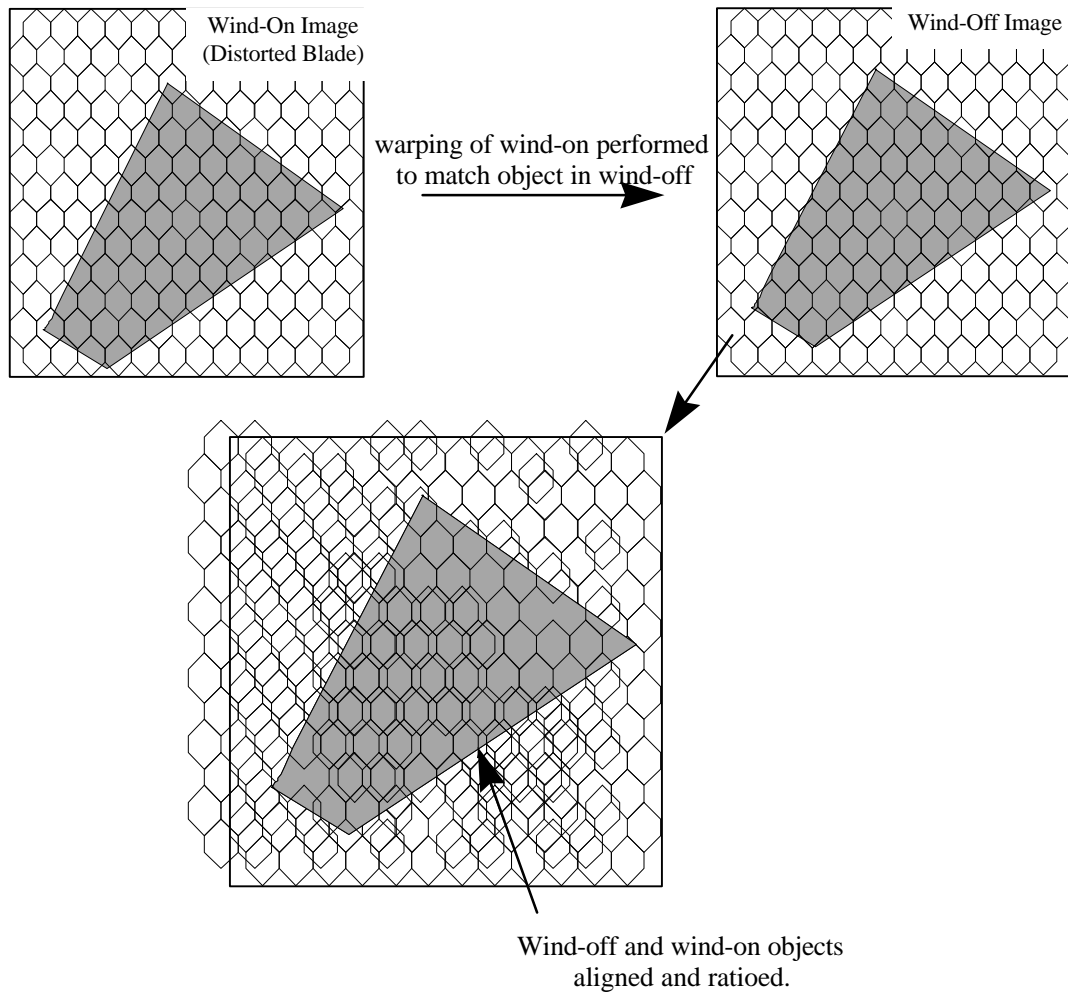

Figure 7.6 Honeycomb-pattern noise caused by ICCD minifier.

To remove the honeycomb pattern caused by the ICCD minifier prior to using PAINTCP, both the background-corrected wind-off and wind-on images were divided by a white image--which was also background corrected. The process is depicted by equation 6:

$$I_{x_{corrected}} = \frac{I_x - I_{black}}{I_{white} - I_{black}} = \frac{(S(x,y)P(x,y)E(x,y) + B(x,y)) - B(x,y)}{(S(x,y)P(x,y)E_0(x,y) + B(x,y)) - B(x,y)} = \frac{E(x,y)}{E_0(x,y)} \qquad (6)$$

where x represents either the wind-off or wind-on condition and the white image records the sensitivity, illumination power, and a reference emission, $E_o(x,y)$. All of the images (white, wind-off, and wind-on) were corrected for thermal noise, $B(x,y)$, by subtracting the background image, I_{black}. Dividing the wind-off and wind-on images by a white image should effectively remove $S(x,y)$ and $P(x,y)$, leaving only the ratio of the paint emission, $E(x,y)$, and the reference emission used to create the white image, $E_o(x,y)$. Therefore, the final images should be free of the thermal noise caused by the CCD and the honeycomb pattern caused by the fiber-optic coupler of the camera. The reference emission, $E_o(x,y)$, cancels later in post processing when the corrected wind-off image is divided by the corrected wind-on image.

Once the wind-off and wind-on images were corrected, the PAINTCP program was used to locate the alignment marks on the corrected images and the program was used to "warp" the corrected wind-on image to match the pattern of alignment marks in the corrected wind-off image. The wind-off image was then divided by the properly aligned wind-on image, and the final-image ratio is written to an IEEE floating binary file. This procedure was performed twice for each test condition--once for the TSP data and once for the PSP data. In order to temperature-correct the PSP data, the TSP image was also aligned with the PSP image. Therefore, all of the pressure and temperature images were aligned to the same wind-off PSP image.

The output from the PAINTCP program was read into a software package which allowed simple matrix and image manipulation. The equation determined from the paint calibration for the TSP was applied to the temperature matrix to convert the intensity ratio to surface temperatures (in ° C). These results were output to a new matrix. Because the temperature image was aligned with the pressure image using PAINTCP, the temperature image could be used to calibrate the pressure image directly. The surface-temperature information and the intensity-ratio data from the PSP image were input into the calibration equation for the PSP, and the resulting surface-pressure information was output to a second matrix. The final temperature image and temperature-corrected pressure image were scaled and plotted with false-color.

29

CHAPTER 8.0   TRANSONIC-ROTOR TEST RESULTS

Figure 8.1 depicts the area of the blade where temperature and pressure data were acquired. The lines are used to outline the physical image region of the blade because the photograph of the blade was taken at a different point-of-view than the data acquired from the paints. The approximate dimensions of the viewable area of the blade where data were acquired are from 0-52% chord at the tip and from 62-100% span at the leading edge. Approximately 61,500 pixels were focused on the blade for P/TSP measurements. Accounting for pixel blur, the actual spatial resolution obtained was 1.2 mm in the direction of rotation and 0.4 mm radially (see Appendix A). Therefore, the PSP offers a measurement point ~ 27% of the size of a 1.5-mm diameter transducer. While the spatial resolution was maintained in the radial direction, only 1/3 of the resolution was achieved circumferentially; thus, the 61,500 pixels imaging the blade provided ~20,500 adjacent measurement points.
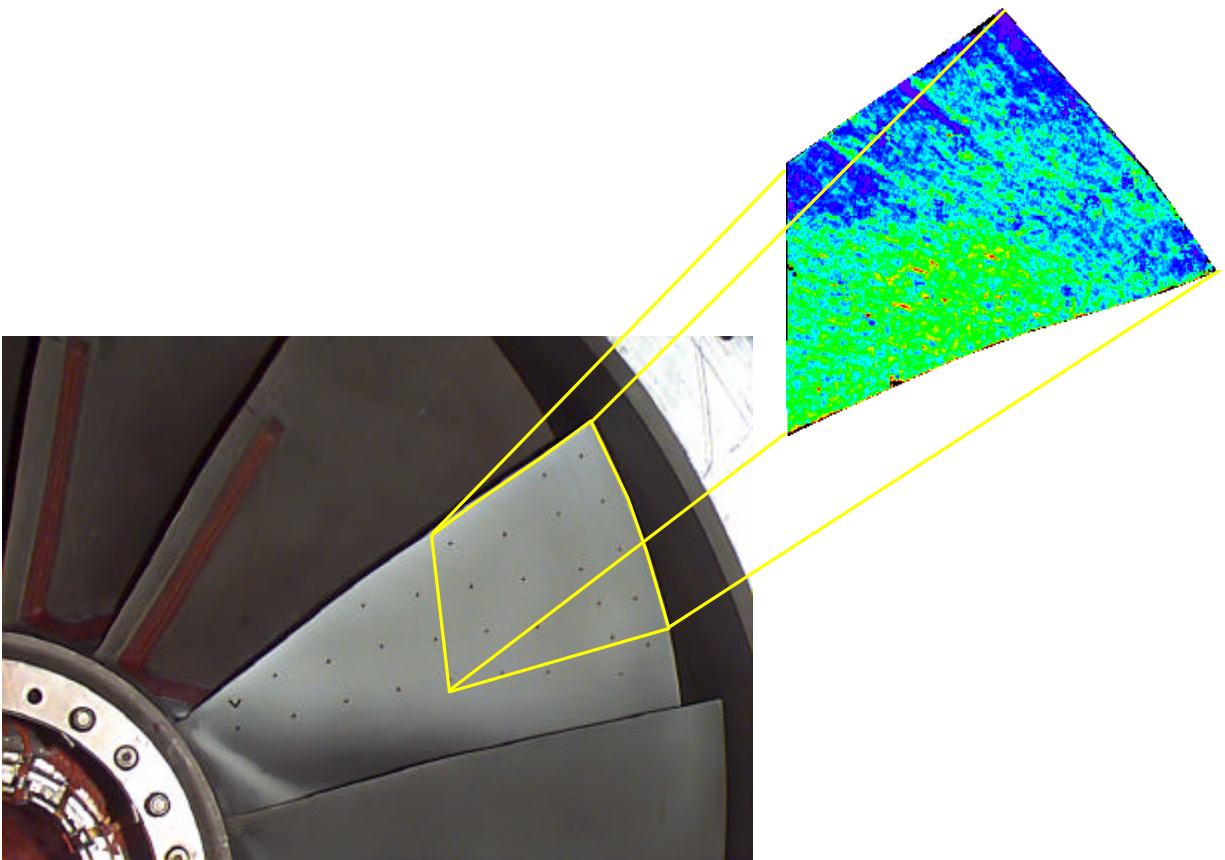

Figure 8.1 First-stage-rotor image region.

The average of fifteen TSP wind-on gray-scale images obtained at the 85% Nc, peak-efficiency condition are presented in Fig. 8.2. The blade-leading-edge tip is located in the upper-right corner and rotates counterclockwise in the image. The flat-field correction was not applied to Fig. 8.2, and the honeycomb pattern which results from the noise can be observed; note the two lines present at the blade tip in the TSP image. These will be addressed later in this section.
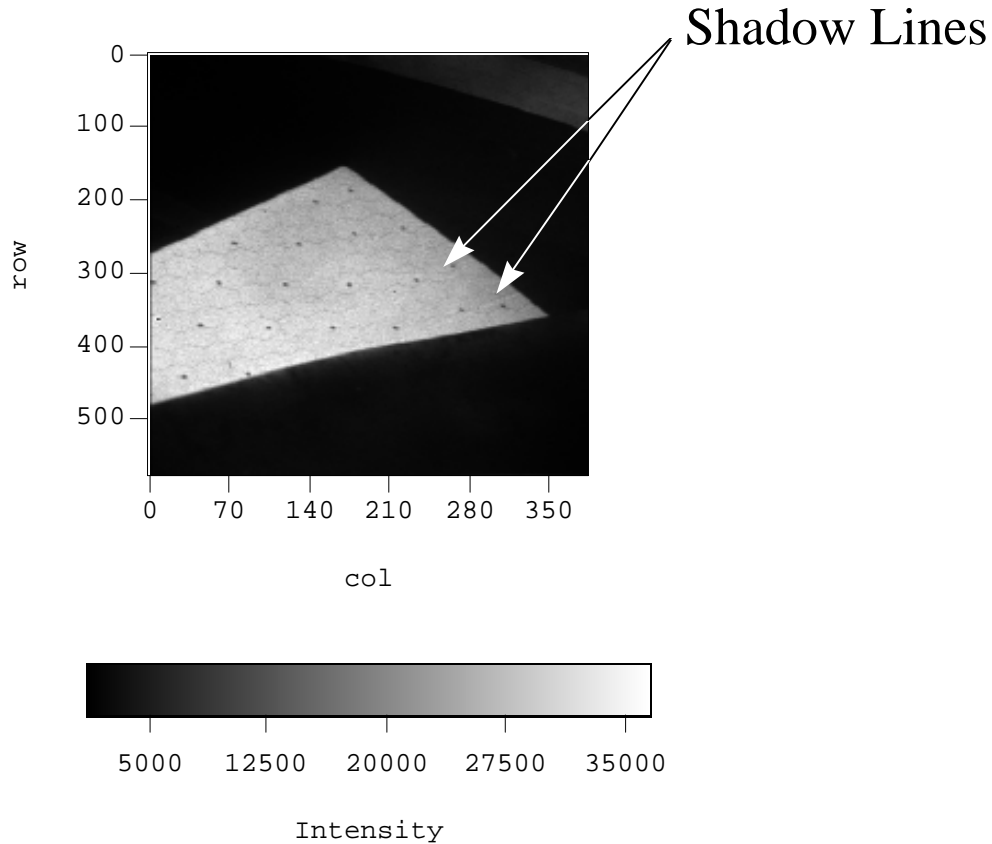

Figure 8.2 TSP wind-on image, 85% Nc, peak-efficiency operating condition, displaying honeycomb-noise pattern.

Evaluation of the preliminary PSP data revealed a troublesome problem. In this data, the honeycomb pattern caused by the minifier attenuation was not successfully removed via flat-field correction. Further evaluation of the camera revealed that the ICCD intensifier was damaged resulting in the degeneration of the linear dynamic range of the camera. Because the failure was not catastrophic, the damage was not apparent prior to the test. Throughout the course of this experiment, six Princeton Instruments ICCD cameras were used; two containing EEV CCD chips and four containing Thompson CCD chips. While both of the ICCDs containing the EEV chips tested normal, all four of the ICCDs containing the Thompson CCD chips no longer exhibited a linear dynamic range. Therefore, it was hypothesized that the Princeton Instruments ST-138

31

camera controller used to drive the ICCDs damaged the intensifier of each camera containing the Thompson CCD chip. The correlation between the specific camera intensifier and the resulting failure is still under investigation.

In an attempt to retrieve the data, the camera response to known intensities was evaluated. Figure 8.3 presents the data from the degraded camera in terms of counts measured by the camera versus actual counts. According to the data, the camera response became non-linear at ~20,000 counts and at 30,000+ counts the camera deviation from linearity was severe. Fortunately, all the data for the PSP displayed counts on the order of 20,000 counts and the TSP data displayed counts on the order of 25,000 counts. Therefore, the non-linearity of the camera response was modeled and a correction factor was applied to each raw PSP and TSP image used for post-processing.
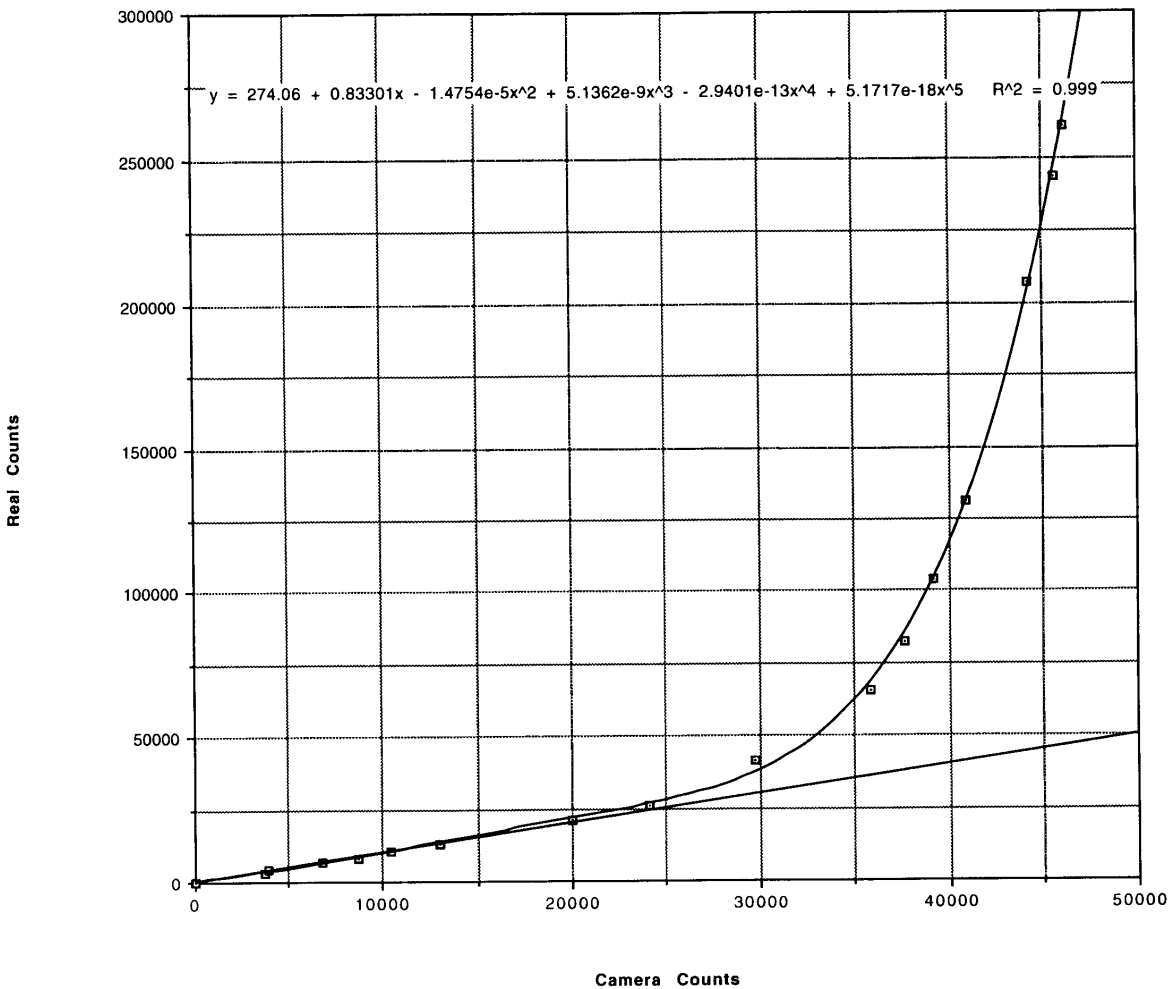

Figure 8.3 Calibrated ICCD dynamic range.

The equation shown in the figure is:

$$y = 274.06 + 0.83301x - 1.4754e\text{-}5x^2 + 5.1362e\text{-}9x^3 - 2.9401e\text{-}13x^4 + 5.1717e\text{-}18x^5 \quad R^2 = 0.999$$

Figures 8.4 presents the final TSP results obtained using the post-processing procedure described above. The surface temperatures at the leading edge ranged from 25° C at ~62% span to 50° C at the tip. At ~52% chord the temperatures ranged from 0° C at ~ 62% span to 50° C at the tip. The lines which were noted in Fig. 8.4 are vaguely noticeable in the final TSP image. These lines can not be considered shockwaves due to the absence of a temperature gradient in the final TSP image. Therefore, it was hypothesized that these lines were the result of variations in the index of refraction of air along the optical path of the camera; these lines represent a shadowgraph of a passage shockwave which created a temperature jump, hence, a sudden change in the index of refraction.
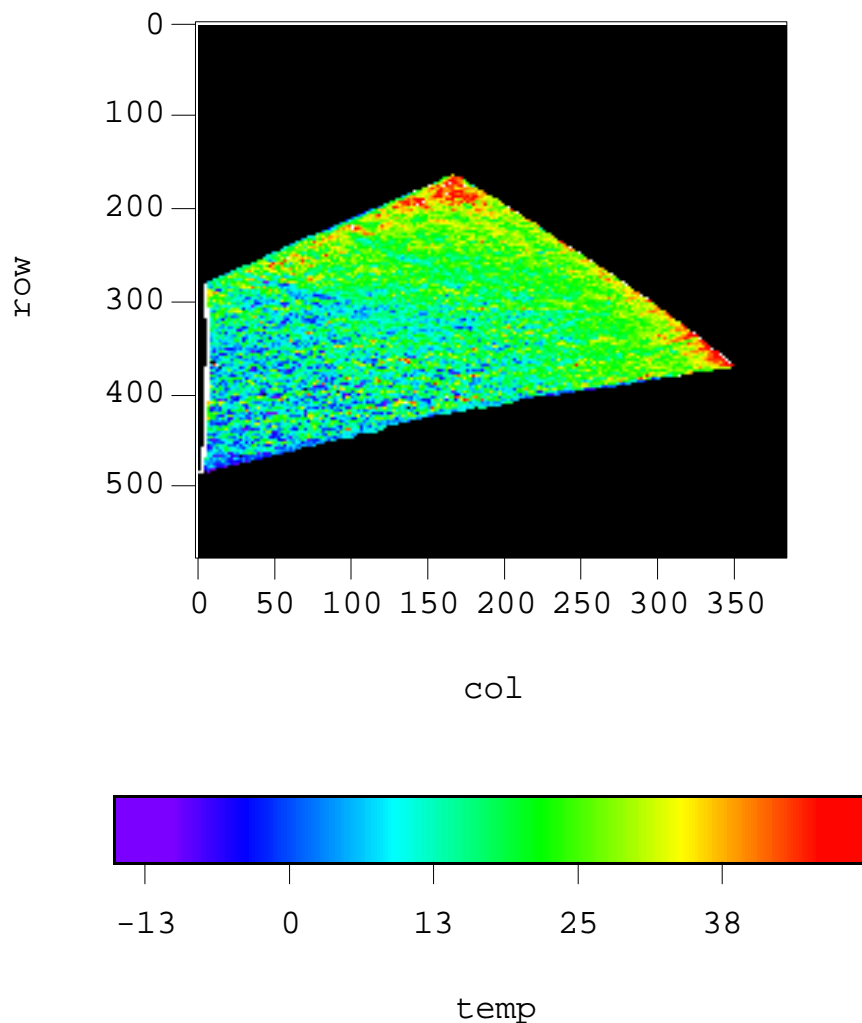

Figure 8.4 Calibrated TSP image at 85% Nc, peak-efficiency operating condition.

The TSP data were used to correct the PSP data, presented in Fig. 8.5. The pressure gradient clearly indicates the presence of a shockwave. Unfortunately, the particular test article studied had a substantial oil leak. The two streamwise "streaks" starting from the leading edge were the result of heavy oil present in the TSP wind-off reference image used in data processing. The comparison of the pre- and post-test wind-off images for both the TSP and the PSP are presented in Appendix C. A slight effect due to photodegradation was apparent in the ratio of the two wind-off images for the PSP. A larger effect was displayed in the TSP comparison as a result of the oil. Generally, the modal distribution of the ratioed images remained one but the post-test wind-off images were used to account for the oil. Unfortunately, this procedure did not completely remove the affect of the oil simply because the oil was not evenly distributed over the entire surface. The streaks displayed in the final PSP image are believed to be areas where the oil was heaviest. As a result, the increased fluorescence in the region falsely indicates higher pressures which show up as streaks in the low pressure region.
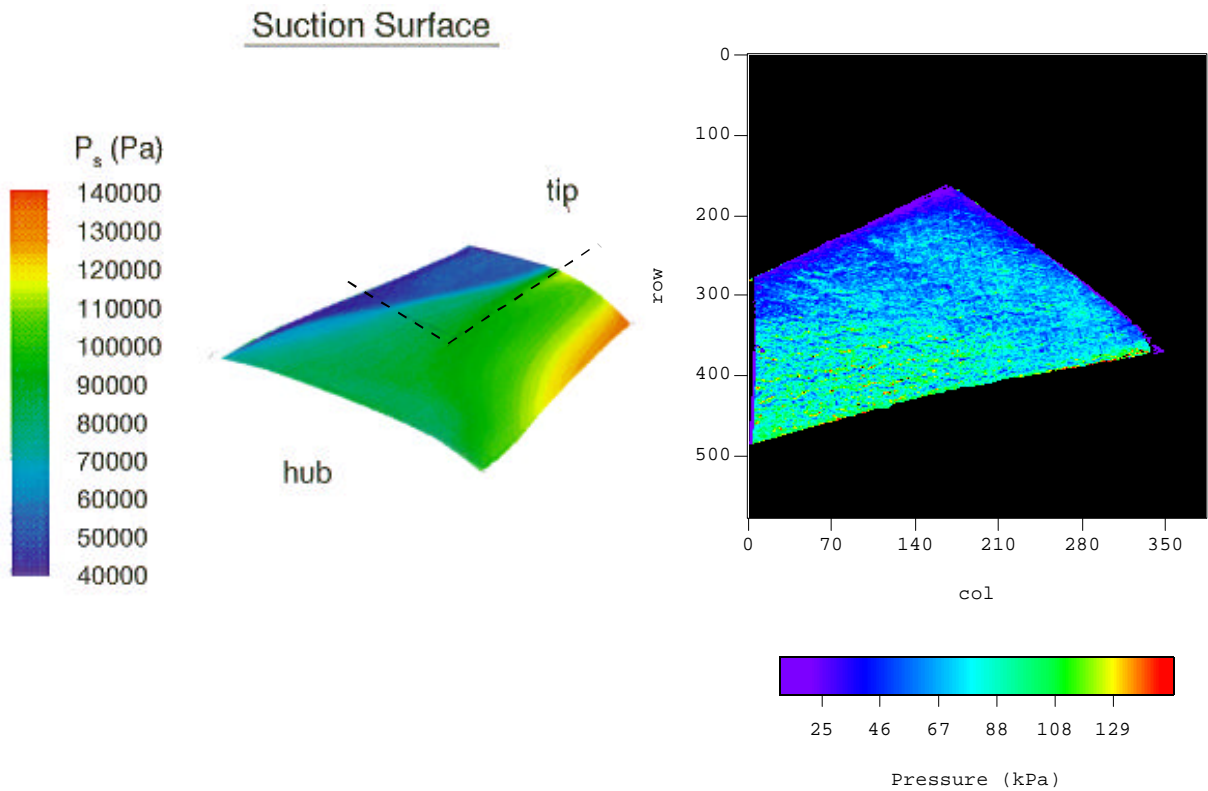

Figure 8.5 CFD prediction and calibrated temperature-corrected PSP image, 85% Nc, peak-efficiency operating condition.

The pressure uncertainties, calculated in Appendix C, increase with both temperature and pressure. Table 8.1 lists the temperature and pressure values along with uncertainty for the final TSP and PSP data for various pixel locations. All of the pixels listed descend along column 168 starting from the tip leading edge of the blade (row 170, column 168). The pixel in row 318 indicates the surface values just before the shock and the remaining pixels indicate surface values after the shock. The CFD prediction presented in Section 5.0 is also shown in Fig. 8.5 for visual comparison; the CFD prediction and the PSP data reveal the general shock position and pressure trends.

Although quantitative data was obtained through the use of a non-linear correction, the consequences of the camera degradation were apparent in the high measurement uncertainties. Also, the inability to remove the honeycomb pattern significantly increased the measurement uncertainty and the camera degradation magnified the measurement errors. While the uncertainty in intensity measurement was expected to be larger for the wind-off and wind-on measurements than for the background and white images, the uncertainties obtained were ~ four times the expected values. The combination of these ballooned errors resulted in exceptionally high measurement uncertainties for both the TSP and the PSP data, as presented in Table 8.1. The uncertainties for the PSP are higher than the uncertainties for the TSP because of the propagation of the TSP uncertainty into the PSP data.

Table 8.1 Measurement values for various pixels along column 168 (starting from the blade leading-edge tip).

Row	Temperature (° C)	Pressure (kPa)
170	42.5±8.1	26.3±5.0
252	16.4±9.1	69.6±18.0
318	16.9±9.1	61.0±16.5
350	19.7±9.0	80.2±19.7
380	12.8±9.2	85.6±21.9
395	8.9±9.4	98.1±24.8

CHAPTER 9.0   CONCLUSIONS

This thesis has described the photophysical properties of luminescent molecules which allows them to be used as pressure-sensing devices. PSP performance requirements for turbomachinery applications have been identified and fluorescence determined to be the

appropriate luminescent process for turbomachinery applications based upon the timing required to image the rotating blade. Development and calibration of fluorescence-based PSPs and TSPs capable of performance up to 2 atm and 150° C have been detailed. The painting procedure, test setup, data acquisition, and post-processing procedures have been presented. The TSP and PSP data acquired from the suction surface of a transonic rotor at 85% corrected speed under the peak-efficiency condition have been presented. Visual comparison of the final PSP image presented in Fig. 8.5 and the CFD prediction presented earlier in Fig. 5.1 reveal similar pressure trends.

Overall, this thesis has demonstrated the potential of using the PSP technique for applications in advanced turbomachinery. Efforts are currently underway to identify more reliable cameras which can be used to acquire rotor data. Future efforts include the modeling of the heat transfer effects of the blade and the paint layer, improved methods of applying the alignment marks, and the further development of paints with increased pressure and temperature capability to accommodate later fan stages. Improvements in pressure sensitivity will rely on the development of probe molecules with improved luminescence quantum efficiency--which will increase the SNR. Future research efforts will be focused on the development of an all-inorganic PSP. Through the synthesis of probe molecules, scientists can control the mechanisms which determine the temperature and pressure capability of the lumiphores used in PSPs. With some inorganic salts having the capability to perform up to 1000° C, inorganic oxygen sensors hold the most promise for the successful development of a PSP for later compressor stages.

REFERENCES

(1)   Sexton, M. R., O'Brien, W. F., and Moses, H. L., "An on Rotor Investigation of Rotating Stall in an Axial Compressor," Defense Technical Information Center (DTIC) Technical Report, Cameron Station, Alexandria, VA, pp. 33.1-10, 1973.

(2)   Peterson, J. I., and Fitzgerald, V. F., "New Technique of Surface Flow Visualization Based on Oxygen Quenching of Fluorescence," *Rev. Sci. Instrum.*, Vol. 51, No. 5, pp. 670-671, 1980.

(3)   Morris, M. J., "Use of Pressure-Sensitive Paints in Low Speed Flows," CH34827-95, IEEE 16th International Congress on Instrumentation in Aerospace Simulation Facilities (ICIASF), Wright-Patterson AFB, OH, 1995, pp.31.1-10.

(4)   Bukov, A. P., Orlov, A. A., Mosharov, V. E., Radchenko, V. N., Pesetsky, V. A., Sorokin, A. V., Phonov, S. D., Alaty, L., and Colucci, V., "Application of Luminescent Quenching for Pressure Field Measurements on the Model Surface in a Wind Tunnel," Wind Tunnels and Wind Tunnel Test Techniques, The Royal Aeronautical Society, Southhampton University, United Kingdom, September 1992.

(5)   Bukov, A., Mosharov, V., Orlov, A., Pesetsky, V., Radchenko, V., Phonov, S., Matyash, S., Kuzmin, M., and Sadozsky, N., "Optical Surface Pressure Measurements: Accuracy and Application Field Evaluation," 73rd AGARD Fluid Dynamics Panel Meeting and Symposium on Wall Interference, Support Interference, and Flow Field Measurements, Brussels, Belgium, 1993.

(6)   Troyanovsky, I., Sadocskii, N., Kuzmin. M., Mosharov, V., Orlov, A., Radchenko, V., and Phonov, S., "Set of Luminescence Pressure-Sensors for Aerospace Research," *Sens. and Act.*, Vol. 11, pp. 201-206, 1993.

(7)   Ardasheva, M. M., Nevskii, L. B., and Pervushin, G. E., "Measurement of Pressure Distribution by Means of Indicator Coatings," *J. Appl. Mech. Tech. Phys.*, No. 4, pp. 24-33, 1985.

(8)   Volan, A., and Alafi, L., "New Optical Pressure Measurement System," IEEE 14th International Congress of Instrumentation in Aerodynamic Simulation Facilities (ICIASF), New York, 1991, pp. 10-16.

(9)   Engler, R. H., Hartmann, K., and Schultze, B., "Aerodynamic Assessment of a New Optical Pressure Measurement System (OPMS) by Comparison with Conventional Pressure Measurements in a High Speed Wind Tunnel," IEEE 14th International Congress of Instrumentation in Aerodynamic Simulation Facilities (ICIASF), New York, 1991, pp. 17-24.

(10) Engler, R. H., "Further Developments of Pressure Sensitive Paint (OPMS) for Non-Flat Models in Steady Transonic Flow and Unsteady Conditions," CH34827-95, IEEE 16th International Congress on Instrumentation in Aerospace Simulation Facilities (ICIASF), Wright-Patterson AFB, OH, 1995, pp. 33.1-8.

(11) "Luminescent Pressure Sensors (LPS) and Luminescent Pressure Sensitive Paints (PSP)," *OPTROD Ltd.*, Dugin str. 17-31, Zhukovsky, Moscow reg., 140160 Russia, 1995.

(12) Bykov, A., Fonov, S., Kishalov, A., Mosharov, V., Orlov, A., Ostroukhov, S., and Radchenko, V., "Application of Luminescent Pressure Sensor Technology to Propellers," Central Aero-Hydrodynamic Institute Internal Document, Preprint No. 99, Moscow, 1995.

(13) Davies, A. G., Bedwell, D., Dunleavy, M., and Brownjohn, N., "Pressure Sensitive Paint Measurements Using Phosphorescence Lifetime Method," 7th International Symposium on Flow Visualization, Seattle, WA, 1995.

(14) Sant, Y. L., and Mérienne, M. C., "An Image Resection Method Applied to Mapping Techniques," CH34827-95, IEEE 16th International Congress on Instrumentation in Aerospace Simulation Facilities (ICIASF), Wright-Patterson AFB, OH, 1995, pp. 46.1-8.

(15) Gouterman, M., Callis, J., Burns, D., Kavandi, J., Gallery, J., Khalil, G., Green, E., McLachlan, B., and Crowder, J, "Luminescence Imaging for Aerodynamic Testing," ONR/NASA Workshop on Quantitative Flow Visualization, J. Sullivan and B. Holmes (eds.), Purdue University, West Lafayette, IN, 1990.

(16) Kavandi, J., Callis, J., Gouternam, M. , Khalil, G., Wright, D., Green, E., Burns, D. , and McLachlan, B., "Luminescent Barometry in Wind Tunnels," *Rev. Sci. Instrum.*, Vol. 61, No. 11, pp. 3340-3347, 1990.

(17) McLachlan, B. G., Bell, J. H., Kennelly, R. A., Schreiner, J. A., Smith, S. C., and Strong, J. M., "Pressure-Sensitive Paint Use in the Supersonic High-Sweep Oblique Wing (SHOW) Test," AIAA-92-2686, AIAA 10th Applied Aerodynamics Conference, Palo Alto, CA, 1992.

(18) McLachlan, B. G., J. H. Bell, J. Gallery, M. Gouterman, and J. Callis, "Boundary Layer Transition Detection by Luminescence Imaging," AIAA Paper No. 93-0177, AIAA 31st Aerospace Sciences Meeting and Exhibit, Reno, NV, 1993.

(19) Harris, J., and Gouterman, M., "Referenced Pressure Sensitive Paint for Flow Visualization VII," 7th International Symposium on Flow Visualization, Seattle, WA, 1995.

(20) McLachlan, B. G., and Bell, J. H., "Pressure-Sensitive Paint in Aerodynamic Testing," *Exp. Thermal Fluid Sci.*, Vol. 10, pp. 470-485, 1995.

(21)   Crites, R. C., Benne, M. E., Morris, M. J., and Donovan, J. F., "Optical Surface Pressure Measurements: Initial Experience in the MCAIR PSTWT," Wind Tunnels and Wind Tunnel Test Techniques, The Royal Aeronautical Society, Southhampton University, United Kingdom, 1992.

(22)   "Pressure-Sensitive Paint: A New Development Tool," *MCAIR Digest*, Vol. 29, No. 3, 1992.

(23)   Hamner, M., B. Campbell, T. Liu, and J. Sullivan, "A Scanning Laser System for Temperature and Pressure-Sensitive Paint," AIAA- Paper No. 94-0728, AIAA 32nd Aerospace Sciences Meeting and Exhibit, Reno, NV, 1994.

(24)   Burns, S., and Sullivan, J., "The Use of Pressure Sensitive Paint on Rotating Machinery," CH34827-95, IEEE 16th International Congress on Instrumentation in Aerospace Simulation Facilities (ICIASF), Wright-Patterson AFB, OH, 1995, pp.32.1-14.

(25)   Liu, T., Johnston, R., Torgerson, S., Fleeter, S., and Sullivan, J., "Rotor Blade Pressure Measurement in a High Speed Axial Compressor using Pressure and Temperature Sensitive Paints," AIAA Paper No. 97-0162, AIAA 35th Aerospace Sciences Meeting and Exhibit, Reno, NV, 1997.

(26)   Jagharhi, A. J., Mitchell, M., Burkett, C., and Sealey, S., "Wind Tunnel Application of Pressure Sensitive Paints at NASA Langley Research Center (8 foot TPT & 7'x10' HST)," NASA LaRC IRD ATMB, NASA Langley Research Center, Hampton, VA, 1993.

(27)   Oglesby, D. M., Upchurch, B. T., Leighty, B. D., and Simmons, K. A., "Pressure Sensitive Paint with Internal Temperature Sensing Lumiphore," 42nd International Instrumentation Symposium, Instrument Society of America, San Diego, CA, 1996.

(28)   Carroll, B. F., Winslow, A., Abbitt, J., Schanze, K., and Morris, M. M., "Pressure Sensitive Paint: Application to a Sinusoidal Pressure Fluctuation CH34827-95, IEEE 16th International Congress on Instrumentation in Aerospace Simulation Facilities (ICIASF), Wright-Patterson AFB, OH, 1995, pp. 35.1-6.

(29)   Hubner, J. P., Abbitt, J. D., and Carroll, B. F., "Pressure Measurements on Rotating Machinery using Lifetime Imaging of Pressure Sensitive Paint," AIAA Paper No. 96-2934, 32nd AIAA/ASME/SAE/ASEE Joint Propulsion Conference and Exhibit, Orlando, FL , 1996.

(30)   Sellers, M. E., and J. A. Brill, "Demonstration Test of Pressure-Sensitive Paint in the AEDC 16 ft Transonic Wind Tunnel Using the TST Model," AIAA Paper No. 94-2481, AIAA 18th Aerospace Ground Testing Conference, Colorado Springs, CO, 1994.

(31)   Sabroske, K. R., Rabe, D. C., and Williams, C., "Pressure-Sensitive Paint Investigation for Application in Turbomachinery," ASME Paper No. 95-GT-92, ASME International Gas Turbine and Aeroengine Congress and Exposition, Houston, Texas, 1995.

(32)   Bencic, T., "Experiences Using Pressure-Sensitive Paint in NASA Lewis Research Center Propulsion Test Facilities," AIAA Paper No. 95-2831, 31st AIAA/ASME/SAE/ASEE Joint Propulsion Conference and Exhibit, San Diego, CA, 1995.

(33)   Kautsky, H., "Quenching of Luminescence by Oxygen," Trans. of the Faraday Society, No. 35, 1939, pp. 216.

(34)   Ingle, J. D. Jr., and Crouch, S. R., Spectrochemical Analysis, Prentice Hall, New Jersey, Ch. 12, 1988, pp. 338-351.

(35)   Schulman, S. G., ed., Molecular Luminescence Spectroscopy. Methods and Applications: Part 2, Ch. 3, 1988, pp. 212-241.

(36)   Russler, P., Rabe, D., Cybyk, B., and Hah, C., "Tip Flow Fields in a Low Aspect Ratio Transonic Compressor," ASME Paper No. 95-GT-089, ASME International Gas Turbine and Aeroengine Congress and Exposition, Houston, Texas, 1995.

(37)   Copenhaver, W. W., Hah, C., and Puterbaugh, S. L., "Three-Dimensional Flow Phenomena in a Transonic, High-Through-Flow, Axial-Flow Compressor Stage," *J. Turbomachinery*, Vol. 115, No. 2, pp. 240-248, 1993.

(38)   Russler, P., "Acquisition and Reduction of Rotor Tip Static Pressure Transducer Data From a Low Aspect Ratio Transonic Fan," Wright Laboratory Technical Report WL-TR-95-2022, Wright Laboratory, Wright-Patterson Air Force Base, OH, 1995.

(39)   Rabe, D., Bölcs, A., and Russler, P., "Influence of Inlet Distortion on Transonic Compressor Blade Loading," AIAA Paper No. 95-2461, 31st AIAA/ASME/SAE/ASEE Joint Propulsion Conference and Exhibit, San Diego, CA, 1995.

(40)   Torgerson, S., Liu, T., and Sullivan, J., "Use of Pressure-Sensitive Paints in Low-Speed Flows," 19th AIAA Advanced Measurement and Ground Testing Technology Conference, New Orleans, LA, 1995.

(41)   James, D. R. , Liu, Y. S., De Mayo, P., Ware, W. R., "Distributions of Fluorescence Lifetimes: Consequences for the Photophysics of Molecules Absorbed on Surfaces," *Chem. Phys. Letters*, Vol. 120, No., 4-5, 1985.
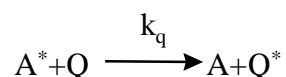
(42)   Liu, Y. S., and Ware, W. R., "Photophysics of Polycyclic Aromatic Hydrocarbons Absorbed on Silica Gel Surfaces. 1. Fluorescence Lifetime Distribution Analysis: An Ill-Conditioned Problem," *J. Phys. Chem*., Vol. 97, pp. 5980-5986, 1993.

(43)   Xu, W., Demas, J. N., DeGraff, B. A., and Whaley, M., "Interactions of Pyrene with Cyclodextrins and Polymeric Cyclodextrins," *J. Phys. Chem*., Vol. 97, pp. 6546-6552, 1993.

(44)   Xu, W., McDonough, R. C., Langsdorf, B., Demas, J. N., and DeGraff, B. A., "Oxygen Sensors Based on Luminescence Quenching: Interactions of Metal Complexes with the Polymer Supports," *Anal. Chem*., Vol. 66, pp. 4133-4140, 1994.

(45)   Aldrich Handbook of Fine Chemicals: 1996-1997, Aldrich Chemical Co., Milwaukee, Wis., pp. 1277.

(46)   Handbook of Chemistry and Physics, 67th ed., CRC Press, 1986-1987, pp. F-89.

(47)   *PaintCp V2.2 User s Guide*, Sterling Software Technical Note TN-93-8006-000-48, 1994.

APPENDIX A: Timing Requirements for Imaging

The gate time required to image the blade is calculated in this appendix. Two factors must be considered: 1) the fluorescence decay, and 2) the acceptable pixel blur. The time of the excitation and the subsequent lifetime of the paint must occur within the data acquisition time (gate time) required to image the rotating blade at a desired spatial resolution. The following sections present the mathematical representation of dynamic quenching used to calculate the lifetime requirements of the paint and the calculation of the gate time required to image the blade given a desired spatial resolution.

Proof of Exponential Decay of Luminescence

The transfer of energy from an excited state lumiphore, A*, to an unexcited quenching molecule, Q, can be described as follows:

$$A^* + Q \xrightarrow{\ k_q\ } A + Q^*$$

where the asterisks denote excited states and k_q is the rate at which the energy is transferred from the lumiphore to the quencher. A mathematical expression can be written to describe the process as follows:

$$\frac{dA^*}{dt} = -k_q [A^*][Q]$$

where the negative sign accounts for the fact that the luminescence intensity of the lumiphore decreases over time. Separating the equation for A* yields:

$$\frac{dA^*}{[A^*]} = -k_q [Q] dt$$

Integrating both sides over a time zero to t yields the desired result:

$$\int_0^t \frac{dA^*}{A^*} = \int_0^t -k_q [Q] dt$$

$$\ln \frac{A^*(t)}{A_0^*} = -k_q [Q(t)]$$

$$\frac{A^*(t)}{A_0^*} = e^{-k_q [Q(t)]}.$$

Figure A.1 presents a plot of the resulting decay as a fraction of an arbitrary lifetime (τ_0) of a lumiphore, which is typically defined as 1/e. As the figure indicates, 5 times the lifetime value is required to collect >99% of the luminescent signal.
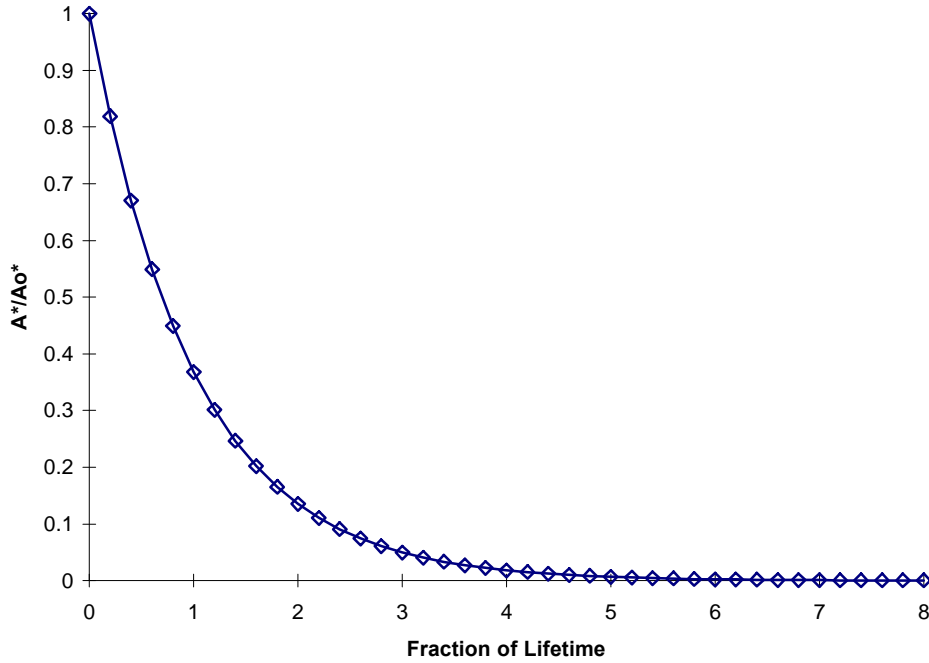

Figure A.1. Normalized luminescent decay versus the fraction of an arbitrary lifetime.

Gate-Time Calculation for Imaging

      The spatial resolution of the system is defined by the camera pixel size and the imaging optics which cause magnification. The timing requirement involves the gate time required to maintain the pixel blur to an acceptable level. The following calculation derives the gate time required to achieve a spatial resolution (image pixel size) of 1 mm.

$$\Delta X_b = N(\frac{1\,\text{min}}{60\,\text{s}})\frac{2\pi}{\text{revolution}}R\Delta t < n\Delta X_p$$

$$\Delta t < \frac{nX_p}{2\pi NR}(\frac{60\,\text{s}}{1\,\text{min}})$$

where,

N	Rotor mechanical speed, rpm (13,288 rpm at 100% Nc)	
R	Rotor radius, m (0.3524 m at the tip)	
Δt	Gate time, s	
ΔX_b	Blade movement during Δt, m	
X_p	Image pixel size, m (0.001 m)	
n	fraction of allowed movement within Δt, (10%)	

Preliminary calculations assumed the blade movement was limited to 1/10 the size of the pixel image. The image pixel is the scale of the CCD pixel size as it is projected on the blade where the physical size of the image pixel depends upon the magnification of the optical system. Using the maximum speed (tip speed at 100% corrected speed), the gate time required to minimize the blur of an assumed 1-mm image-pixel size to 0.1 mm was calculated to be < 2 µs. As a result of this timing requirement to image the blade, the lifetime of the lumiphore used must be $1/5^{th}$ the gate time, or < 400 ns, as presented in Section 5.1 and above.

The actual size of the image pixel achieved and the number of pixels imaging the blade were determined from a wind-off image of the PSP data. Knowledge of the dimensions of the alignment mark locations which appeared in the image allowed for the calculation of the scale of the CCD pixel. The size of the image pixel was determined to be 0.4 mm and the scale, or magnification, based upon the square CCD pixel of 22.5 μm^2 was determined to be ~84. The number of image pixels on the blade were then physically counted; a total of 61,500 pixels imaged the painted blade. With a leading edge blade height of ~0.22 m and a tip chord of ~0.21 m, the imaged region of the blade was determined to be from 62-100% span along the leading edge and 0 - 52% chord along the tip.

With the actual size of the image pixel being much smaller than the estimated size, the blur was not limited to 0.1 mm. The data presented in this thesis were obtained at 85% corrected speed (11,294.8 rpm) and the blade tip moved 0.67 mm during the achieved gate time of 1.6 µs ($5\tau_0$). Therefore, the actual spatial resolution obtained was one pixel in the radial by one pixel plus the blade movement in the direction of rotation, or 0.4 by 1.2 mm (rounding to the next pixel). Therefore, PSP offers a measurement point 27% of the size of a typical 1.5-mm diameter transducer. While the spatial resolution was maintained in the radial direction, only 1/3 of the resolution was achieved circumferentially; thus, the 61,500 pixels imaging the blade provided ~20,500 adjacent measurement points. The spatial resolution was limited by the PSP because the lifetime of the PSP was larger than that of the TSP.

APPENDIX B: Previous PSP Applications in Turbomachinery

A low-speed demonstration of PSP data acquisition was conducted in August of 1994 at the Wright Laboratory Turbine Engine Research Center (TERC). Qualitative data were acquired from the suction surface of a subsonic high-aspect-ratio fan blade. A back-illuminated CCD camera was used in conjunction with an optical derotation device for imaging the rotating blade. The details of the experimental test setup and the optical derotator can be found in reference 31. Figure B.1 shows the wind-on image acquired from the fan rotating at 1,500 rpm. The CCD camera and lens system allowed ~10,000 measurement points on the blade surface. Each pixel measured the light intensity emitted from the blade and represented a potential pressure-measurement location on this blade during rotation. In the figure the hub is located at the top left and the tip of the blade at the lower right. The direction of rotation is clockwise in this view. The light areas correspond to the highest intensities (low pressures) and the dark areas to the lowest intensities (high pressures). This trend in intensity can be seen more clearly in the chord-wise plot of the blade shown in Fig. B.2; the black line in Fig. B.1 indicates the location of the slice. If one remembers that the pressure is inversely related to the intensity, Fig. B.2 clearly shows that the pressure at first decreases and then increases along the chordline, as expected on the suction surface of a subsonic airfoil. Paint developed by Arnold Engineering Development Center (AEDC) was used in this experiment. Quantification of these data was not possible because the wind-off and wind-on images could not be sufficiently aligned during post-processing.
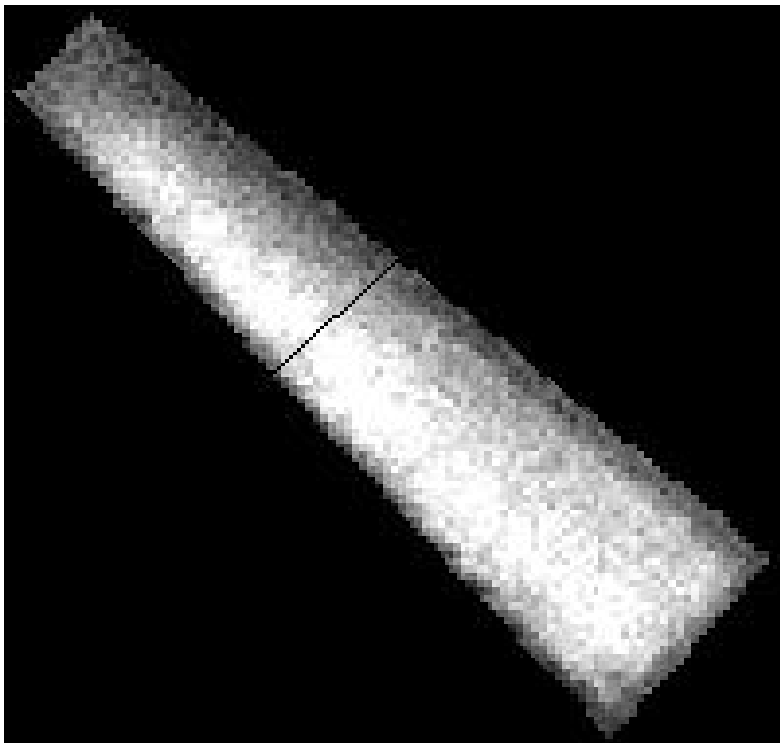

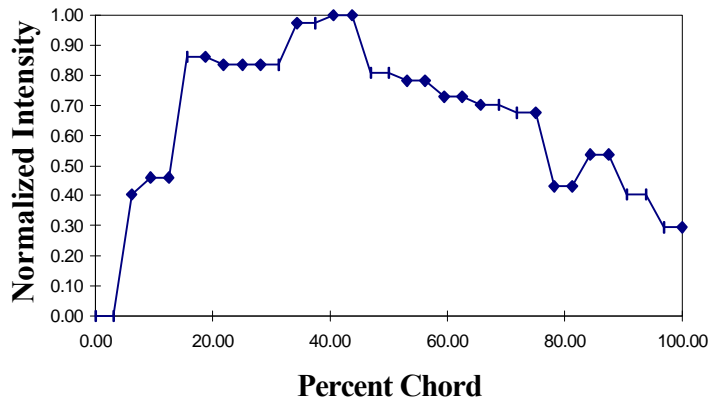**Figure B.1** Wind-on intensity measurement at 1,500 rpm.

Figure B.2 Plot of normalized intensity vs. percent chord on the suction surface.

A follow-on experiment was conducted at the TERC on a full-scale transonic rotor in March of 1996. The technique employed in the low-speed demonstration was used; however, a gated, intensified CCD (ICCD) camera and pulsed laser were used to image the blade. In this test, the beam generated by a small (300-μJ, 3-ns) pulsed nitrogen laser was expanded to illuminate the blade surface for paint excitation. The once-per-revolution signal triggered both the laser and the camera. The timing requirement for imaging the rotating blade, calculated in Appendix A, was determined to be a 2-μs window. Thus, a paint with a fast luminescent-decay time, or fluorescent paint, was used. Unfortunately, most of the paints (including the AEDC paint used in the previous rotor experiment) available at that time utilize the slower phosphorescent process to optimize pressure sensitivity. The only fluorescent paint commercially available was the LPS-2 made by TsAGI [11]. Therefore, only two paints were used in the first transonic rotor test, the LPS-2 obtained from TsAGI and a paint made by WL; both paints employed some form of pyrene. Figure B.3 shows the painted blades of the test article.

The laser and ICCD camera shared a common access port, located 2 ft upstream of the rotor at -10 deg off top dead center. The port was 12.7 mm wide and 50.8 mm long. The camera imaged the blade across the bullet nose in the lower right quadrant. Although both paints adhered to the blade; the TsAGI paint lacked the pressure sensitivity to adequately resolve the flow phenomenon and the WL paint (employing pure pyrene) did not survive the temperature. As the blade temperature increased during a test run the vaporization of the pyrene molecules was apparent as the fluorescence slowly disappeared leaving only the binding medium. The vaporization originated at the tip and propagated towards the hub. Figure B.4 presents a PSP image acquired at 85% Nc at the near-stall operating condition prior to the complete loss of fluorescence; the loss of pyrene is apparent at the tip. Again, quantification of this data was not possible because the wind-off and wind-on images could not be properly aligned.

46

Figure B.3 Painted blades of test article used in preliminary transonic-rotor test.
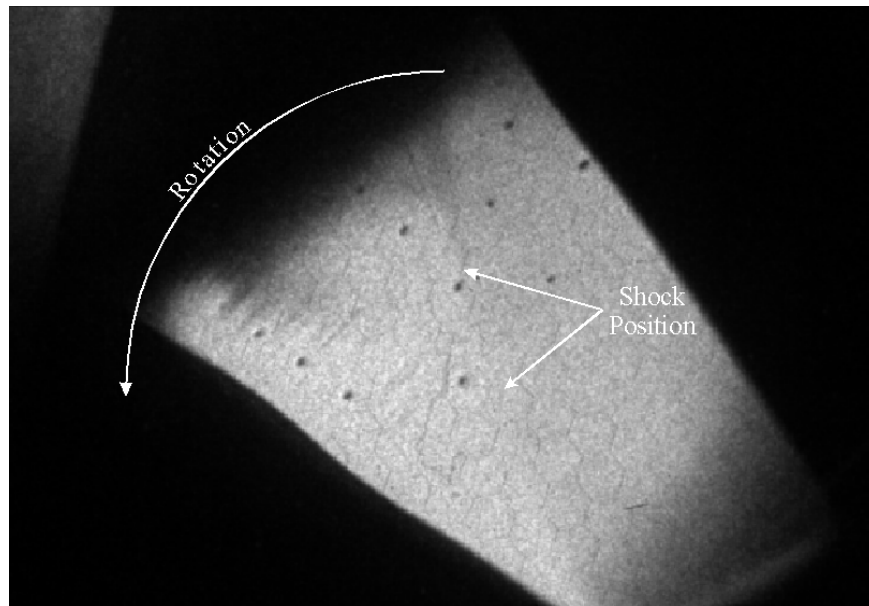

Figure B.4 Qualitative PSP data reveals shock structure at 85% Nc, near-stall operating condition.

APPENDIX C: TSP/PSP Measurement Uncertainty

A simplified analysis of the measurement uncertainty is considered in this section. The TSP measurement uncertainty will be discussed first since an estimate of the temperature uncertainty is required for the PSP uncertainty estimate. The parametric equation for the Wright Laboratory TSP has the form:

$$T = A + B\frac{I_{REF}}{I} + C\left[\frac{I_{REF}}{I}\right]^2$$

where the coefficients A, B, and C are determined through calibration. The corresponding uncertainty in temperature is:

$$\omega_T = \left[\left(\frac{\partial T}{\partial A}\right)^2 \omega_A{}^2 + \left(\frac{\partial T}{\partial B}\right)^2 \omega_B{}^2 + \left(\frac{\partial T}{\partial C}\right)^2 \omega_C{}^2 + \left(\frac{\partial T}{\partial I_R}\right)^2 \omega_{I_R}{}^2\right]^{1/2}$$

where omega represents the respective measurement uncertainties and I_R is a simplified variable which represents the intensity ratio I_{REF}/I. In the application of the TSP, the error associated with the intensity measurement, ω_{I_R}, dominates the uncertainty. Thus, assuming the calibration is arbitrarily good, the TSP uncertainty in temperature measurement reduces to:

$$\omega_T = \left[\left(\frac{\partial T}{\partial I_R}\right)^2 \omega_{I_R}{}^2\right]^{1/2}.$$

The parametric Stern-Volmer equation for the PSP has the form:

$$P = A(T) + B(T)I_R + C(T)I_R{}^2$$
$$A(T) = a_1 + a_2 T + a_3 T^2 + a_4 T^3$$
$$B(T) = b_1 + b_2 T + b_3 T^2 + b_4 T^3$$
$$C(T) = c_1 + c_2 T + c_3 T^2 + c_4 T^3$$

where A(T), B(T), and C(T) are determined through calibration. The corresponding uncertainty in pressure is:

$$\omega_P = \left[\sum_{i=1}^{4}\left\{ \left(\frac{\partial P}{\partial a_i}\right)^2 \omega_{a_i}^{\ 2} \right\} + \sum_{i=1}^{4}\left\{ \left(\frac{\partial P}{\partial b_i}\right)^2 \omega_{b_i}^{\ 2} \right\} + \sum_{i=1}^{4}\left\{ \left(\frac{\partial P}{\partial c_i}\right)^2 \omega_{c_i}^{\ 2} \right\} + \left(\frac{\partial P}{\partial T}\right)^2 \omega_T^{\ 2} + \left(\frac{\partial P}{\partial I_R}\right)^2 \omega_{I_R}^{\ 2} \right]^{1/2}.$$

Here again, the error terms associated with the paint calibration are considered small compared to the error terms associated with the TSP (ω_T) and the intensity measurement; the equation simplifies to:

$$\omega_P = \left[\left(\frac{\partial P}{\partial T}\right)^2 \omega_T^{\ 2} + \left(\frac{\partial P}{\partial I_R}\right)^2 \omega_{I_R}^{\ 2} \right]^{1/2}.$$

To estimate the error in intensity measurement, fifteen images were averaged and the standard deviation was computed on a pixel-by-pixel basis for each paint. The measurement uncertainty, ω_{I_R}, was defined as the standard deviation of the measured intensity divided by the average intensity of each pixel; i.e. the relative standard deviation (RSD). The RSD was determined for the background, white, reference, and test conditions used to produce the final TSP and PSP images; the histograms of the RSD distribution of the 61,500 pixels in each image are presented in Figures C.1 to C.6.

The background intensity image contributes a negligible amount of error as compared to the white, wind-off, and wind-on measurements. The approximate RSD for the white image was 7%--nearly four times the RSD expected for the measurement of a uniformly lit surface. The resulting RSD for the PSP wind-on and wind-off images was ~ 9.0% and for the TSP wind-on and wind-off images RSD was ~ 7.5%. Figures C.7 and C.8 present histograms of the measurement uncertainty for the TSP and PSP according to the above calculation.
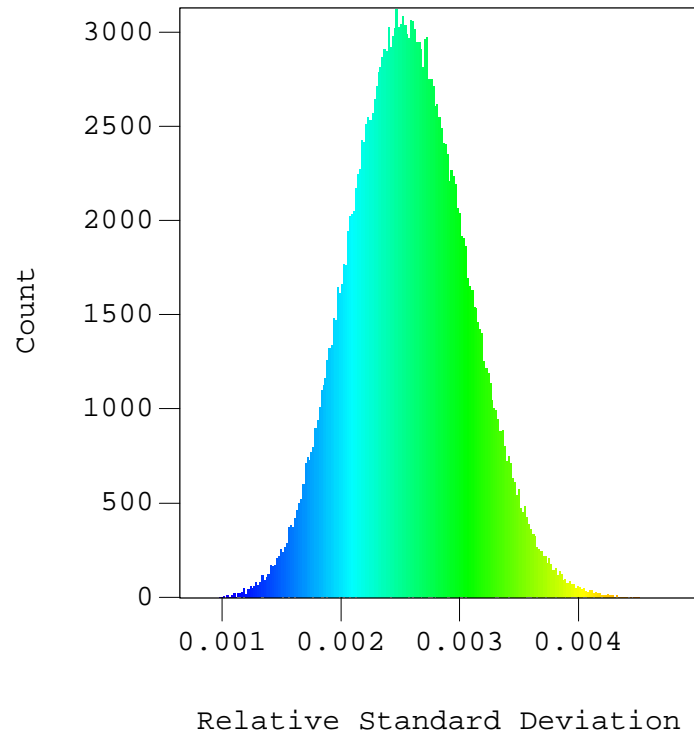
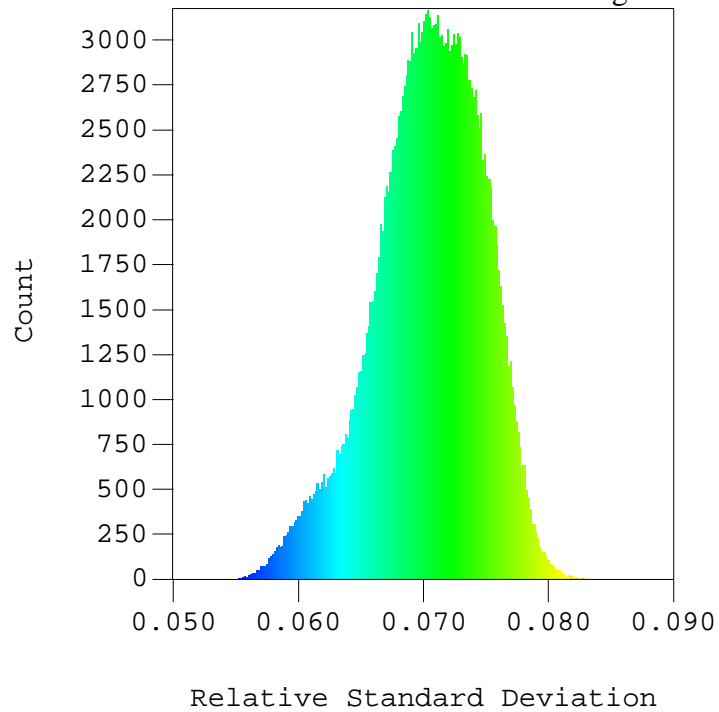**Figure C.1** Histogram of the relative standard deviation for the background image.

Figure C.2 Histogram of the relative standard deviation for the white image.
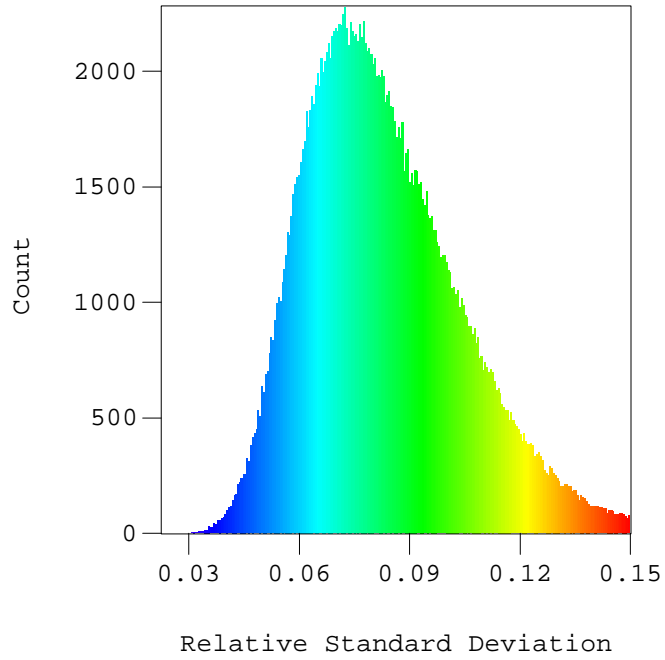
Figure C.3 Histogram of the relative standard deviation for the PSP wind-on image at the 85% Nc, peak-efficiency condition.
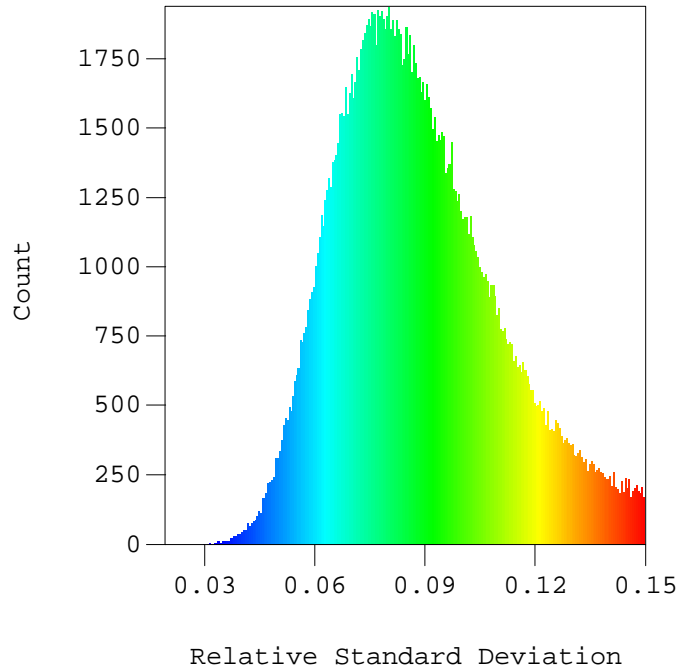

Figure C.4 Histogram of the relative standard deviation for the PSP wind-off image at the 85% Nc, peak-efficiency condition.
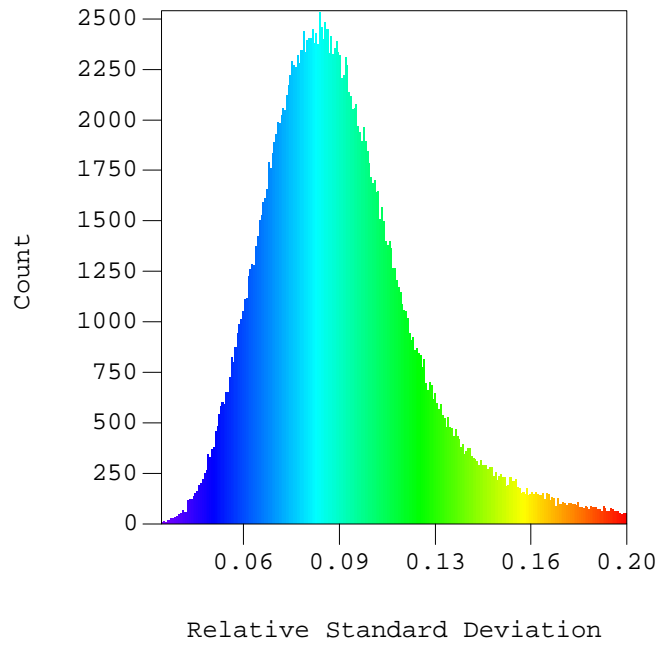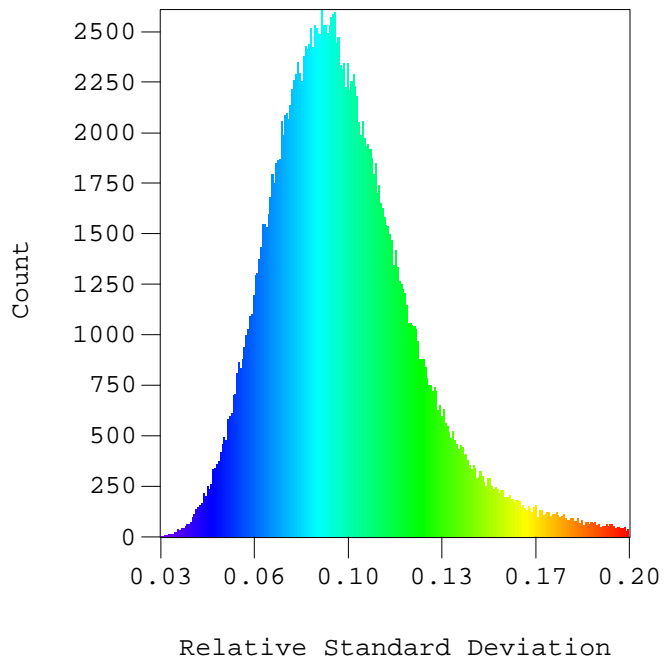
Figure C.5 Histogram of the relative standard deviation for the TSP wind-on image at the 85% Nc, peak-efficiency condition.

Figure C.6 Histogram of the relative standard deviation for the TSP wind-off image at the 85% Nc, peak-efficiency condition.
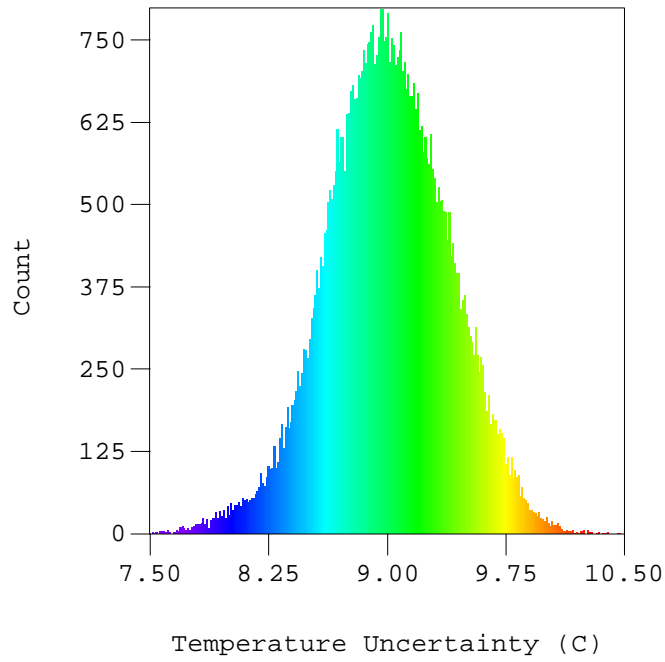
Figure C.7 TSP measurement uncertainty using an estimated 9.0% intensity measurement uncertainty.
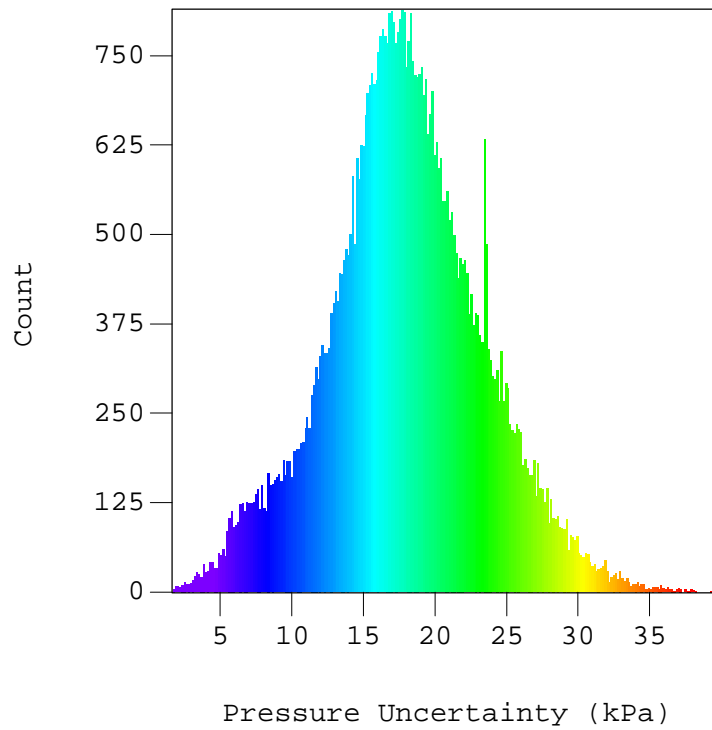

Figure C.8 PSP measurement uncertainty using an estimated 7.5% intensity measurement uncertainty.

Figures C.9 and C.10 present the comparison of the pre- and post-test wind-off images for the PSP data and the TSP data, respectively. The modal distribution of the PSP ratio of the two images was ~1; although the slight increase in counts to the left of the distribution peak was determined to be a result of the photodegradation of the paint. Four hundred and sixty images were acquired between each set of wind-off images resulting in an energy input of 11.1 nJ. The expected paint photodegradation was ~ 2.7% for the PSP and ~ 0.7% for the TSP. The TSP data shows a more dominant bi-modal distribution as a result of the oil streaks which were obviously present in the post-test wind-off image. Unfortunately, the test article had a substantial oil leak. The effect of the oil could not be completely removed because the oil was exceptional heavy in some regions, as noted by the visible streaks in the final PSP image. PAINTCP was not used to align the objects in each of the images used for comparison. Therefore, some of the differences between the images could be the result of a slight shift between the data sets.
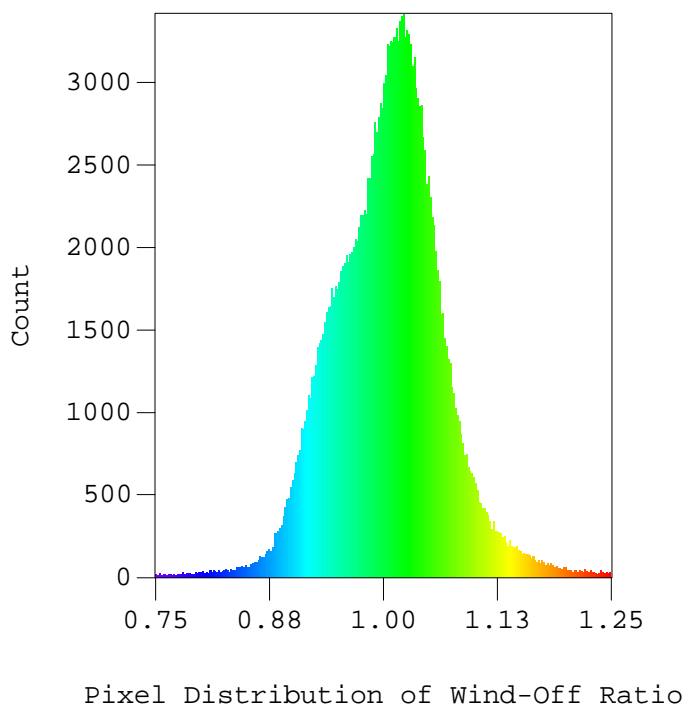

Figure C.9 PSP pre- and post test wind-off comparison.
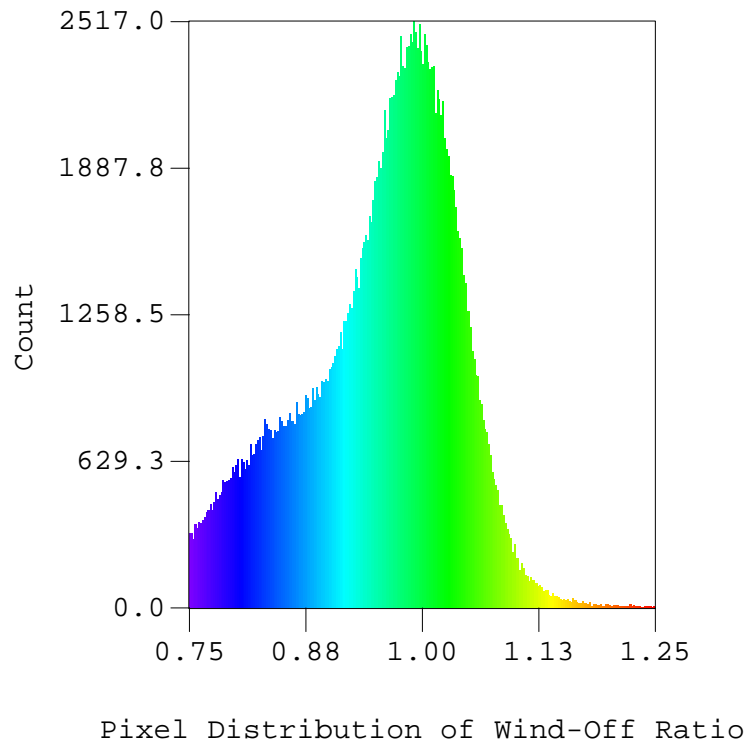
Figure C.10 TSP pre- and post test wind-off comparison.

APPENDIX D: Compressor-Research-Facility Background

Figure D.1 presents the layout of the Turbine Engine Research Center (TERC) Compressor Research Facility (CRF) located at Wright-Patterson Air Force Base. The facility consists of four buildings. Building 71B contains the control facilities and personnel offices, and Building 71D houses the water tower and cooling-water pumps. The test chamber, drive motors, and signal-conditioning room are housed in Building 20A, while the high-voltage equipment and frequency converters needed to power the drive motors are located in Building 20.
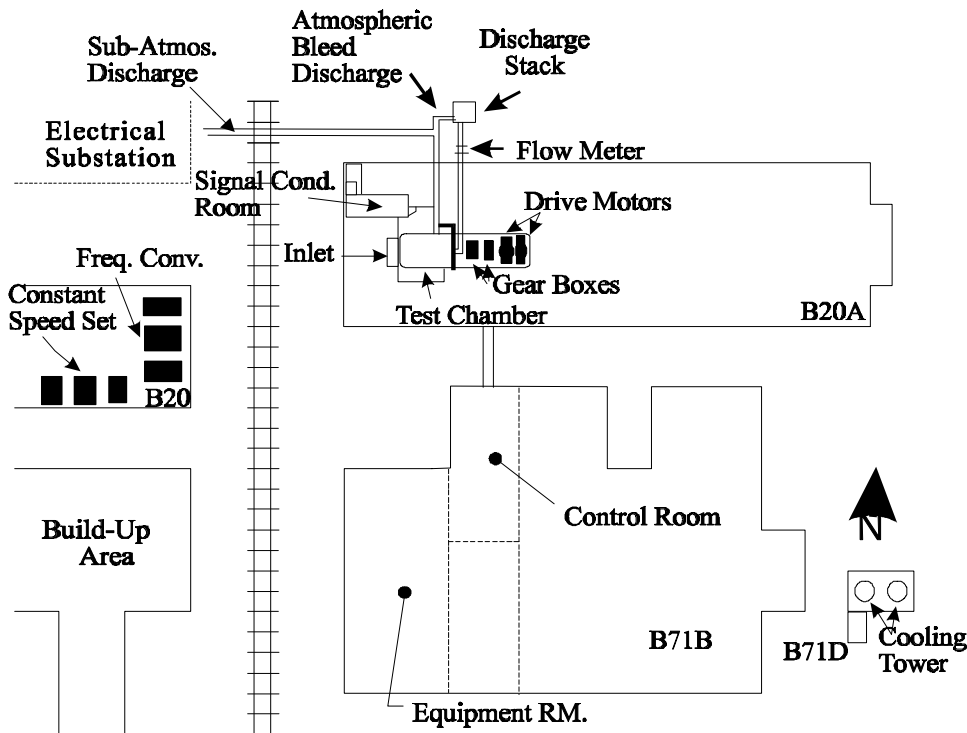

Figure D.1 Layout of the Compressor Research Facility.

The CRF has an open-cycle design in which the test article provides the motive power to move air through the facility. The test article was mounted inside a 19.8-m-long, 6.1-m-diameter test chamber. Atmospheric air enters a plenum upstream of the test article after passing through the inlet filter house and an array of five throttling valves. These valves provide a means of reducing the inlet pressure to the test article. A flow-conditioning barrel mounted inside the plenum contained screens and flow straighteners to minimize distortion. From the plenum the air enters the test article bellmouth and passes through a set of inlet ducts before entering the compressor. The facility can provide airflow rates in the range from 6.8 - 226.8 kg/sec to the test article.

Fan-core discharge flow passes through an instrumented diffuser and a core discharge valve (CDV) before being dumped into the facility exhaust collector. The CDV provides the discharge back pressure necessary for mapping compressor performance. The discharge air flows through a venturi before being exhausted to the atmosphere through a noise-attenuating discharge stack. The compressor test is conducted with a 30-in.-diameter venturi. The CRF powers the test article through an electrical drive system, which results in very accurately fixed rotational speeds. The test-article speed is controlled by varying the frequency of the power provided to the 22.37-MW synchronous electric motor.

VITA

Kelly R. Navarra

Kelly R. Navarra (maiden name Sabroske) was the first of a set of identical twins born in Toledo, Ohio, on September 12, 1970. Raised in a small community just south of Toledo, Kelly graduated from Rossford High School in 1989. Having decided to pursue a degree in engineering, she moved to Dayton, Ohio, to attend the University of Dayton (UD). She graduated from UD in December of 1993 with a Bachelor of Science degree in Mechanical Engineering.

During her sophomore year at UD, Kelly entered the co-op program and was employed at the Wright Laboratory Compressor Research Facility. Continuing as a graduate co-op student, Kelly attended Virginia Polytechnic Institute and State University (VPI&SU) in pursuit of a Master of Science degree in Mechanical Engineering. Leaving VPI, she accepted a position with Innovative Scientific Solutions, Inc. (ISSI), in May of 1996. Her duties at ISSI involve the development of the pressure-sensitive-paint technique for turbomachinery applications. The results of her efforts are presented in this thesis.